



Calhoun: The NPS Institutional Archive DSpace Repository

Theses and Dissertations

1. Thesis and Dissertation Collection, all items

1972

Beam current monitoring and radiachromic film dosimetry at the NPS Linac.

Gray, Frederic Colbert

Monterey, California. Naval Postgraduate School

<http://hdl.handle.net/10945/16008>

This publication is a work of the U.S. Government as defined in Title 17, United States Code, Section 101. Copyright protection is not available for this work in the United States.

Downloaded from NPS Archive: Calhoun



<http://www.nps.edu/library>

Calhoun is the Naval Postgraduate School's public access digital repository for research materials and institutional publications created by the NPS community.

Calhoun is named for Professor of Mathematics Guy K. Calhoun, NPS's first appointed -- and published -- scholarly author.

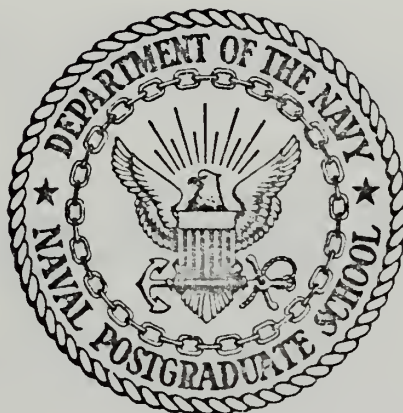
Dudley Knox Library / Naval Postgraduate School
411 Dyer Road / 1 University Circle
Monterey, California USA 93943

BEAM CURRENT MONITORING AND
RADIACHROMIC FILM DOSIMETRY AT THE NPS LINAC

Frederic Colbert Gray

NAVAL POSTGRADUATE SCHOOL

Monterey, California



THESIS

Beam Current Monitoring
and
Radiachromic Film Dosimetry at the NPS Linac

by

Frederic Colbert Gray

Thesis Advisor:

John N. Dyer

June 1972

Approved for public release; distribution unlimited.

Beam Current Monitoring
and
Radiachromic Film Dosimetry at the NPS Linac

by

Frederic Colbert Gray
Captain, United States Army
B. S., United States Military Academy, 1964

Submitted in partial fulfillment of the
requirements for the degree of

MASTER OF SCIENCE IN PHYSICS

from the

NAVAL POSTGRADUATE SCHOOL
June 1972

Thes ~

6716

c.1

ABSTRACT

The beam current monitoring system at the NPS electron Linac was studied to determine its performance under varying conditions of machine operation. The efficiency of the secondary emission monitors (SEM efficiency), defined as the ratio of SEM current of Faraday cup current, was found to increase with increasing beam energy, increase with the introduction of targets into the beam, and vary erratically with SEM foil surface conditions. No dependence on beam current was observed.

The spatial variation of electron fluence (time-integrated flux) was investigated using RACM 203 radiachromic film developed by the EG&G Corporation. The optical density of this film was found to vary linearly with absorbed dose over a range of 5 to 40 megarads. Beam profiles were obtained at 4 locations in the Linac end station for beam energies of 25 and 63 MeV. In addition, the film was used to observe and measure the effect of cascade showers in thick absorbers.

TABLE OF CONTENTS

I.	INTRODUCTION -----	7
II.	FACTORS INFLUENCING THE PERFORMANCE OF SECONDARY EMISSION MONITORS -----	9
A.	THE BEAM CURRENT MONITORING SYSTEM AT THE NPS LINAC -----	9
B.	DESCRIPTION AND THEORY OF OPERATION OF SECONDARY EMISSION MONITORS -----	12
C.	CONDUCT OF THE INVESTIGATION -----	15
D.	SEM EFFICIENCY AS A FUNCTION OF FOIL SURFACE CONDITIONS -----	16
E.	SEM EFFICIENCY AS A FUNCTION OF BEAM ENERGY -----	19
F.	SEM EFFICIENCY AS A FUNCTION OF BEAM CURRENT -----	21
G.	SEM EFFICIENCY AS A FUNCTION OF SEM LOCATION -----	23
III.	INVESTIGATION OF THE LINAC BEAM PROFILE USING RADIACHROMIC FILM DOSIMETRY -----	26
A.	UTILIZATION AND CALIBRATION OF RADIACHROMIC FILM -----	26
1.	Description of Film -----	26
2.	Reading of Radiachromic Films -----	27
3.	Curve Fitting of Optical Density Readings -----	29
4.	Calibration of Films -----	34
B.	INVESTIGATION OF THE LINAC BEAM PROFILE -----	38
1.	Beam Profile as a Function of Location -----	38
2.	Beam Profile as a Function of Absorber -----	39
APPENDIX A	DETERMINATION OF THE EFFECT OF BREMSSTRAHLUNG IN THE TARGET CAUSING PAIR PRODUCTION IN THE SEM FOILS -----	56
APPENDIX B	TABLE OF GAUSSIAN PARAMETERS OBTAINED BY CURVE FITTING OF BEAM PROFILES -----	58

LIST OF REFERENCES -----	60
INITIAL DISTRIBUTION LIST -----	62
FORM DD 1473 -----	63

LIST OF DRAWINGS

1. Schematic of Beam Current Monitoring System-----	10
2. Construction of Sample Secondary Emission Monitor-----	13
3. Variation of SEM Efficiency with Time Elapsed Since Exposure to Air.-----	17
4. Variation of SEM Efficiency with Beam Energy-----	20
5. Variation of SEM Efficiency with Beam Current-----	22
6. Example of Good Fit of Beam Profile to Gaussian-----	31
7. Example of Poor Fit of Beam Profile to Gaussian-----	32
8. Example of Non-linear Film Response-----	33
9. Collision Stopping Power and Dose Conversion Factor for Polyethylene as Functions of Beam Energy -----	36
10. Relationship Between Absorbed Dose and Radiachromic Film Optical Density -----	37
11. Representative Beam Profiles at Target Plane-----	40
12. Representative Beam Profile at Radiation Damage Site-----	41
13. Example of Non-Symmetry of Target Ladder Beam Profiles-----	42
14. Example of Non-isotropy of Beam Profile, Exit Window, 63 MeV-----	43
15. Example of Non-isotropy of Beam Profile, Radiation Damage Site, 63 MeV -----	44
16. Example of Non-Isotropy of Beam Profile, Exit Window, 25 MeV-----	45
17. Example of Non-Isotropy of Beam Profile, Radiation Damage Site, 25 MeV -----	46
18. Comparison of Beam Profiles at Three Sites Outside Target Chamber, 63 MeV -----	47
19. Comparison of Beam Profiles at Three Sites Outside Target Chamber, 25 MeV -----	48
20. Angular Dispersion of Beam Past Target Plane -----	49
21. Beam Profiles Before and After Lead Slab, 25 MeV -----	51

22. Beam Profiles Before and After Beryllium Slab, 25 MeV-----	52
23. Beam Profiles Produced in Lead Stack, 63 MeV-----	53
24. Beam Profiles Produced in Beryllium Stack, 63 MeV-----	54
25. Effect of Absorber Thickness on Total Electrons-----	55

I. INTRODUCTION

During the period June 1971 to June 1972, the electron Linac at the Naval Postgraduate School was used primarily for two distinct classes of experiment; the study of radiation damage in semiconductor devices, and high precision nuclear scattering. The investigations described in this thesis were initiated to improve the accuracy and reliability of results obtained by these two experimental procedures by improving the knowledge and understanding of the beam electron fluence as function of machine operating conditions.

Both experiments demand knowledge of the fluence expressed as the total number of electrons passing through a particular area in a given time period. For nuclear scattering, the exact number of electrons striking a target had to be known as precisely as possible. The attainment of one per cent accuracy in the scattering results demanded considerably better accuracy in the measurement of the total number of electrons. However, since the targets were large compared to the beam cross-section, the spatial variation of the electron fluence across that cross-section was of little concern. This was not the case for the radiation damage studies. The active area of the semiconductor devices irradiated was much smaller than the beam cross-section. Determination of the number of electrons passing through this active area thus required the knowledge of the spatial variation of electron fluence. The radiation damage studies did not require the high precision demanded by the nuclear scattering experiments.

These two problems, though related, required two separate and distinct investigations. Improving the knowledge and understanding of the total number of electrons passing through a large target involved the study of the beam current monitoring system and its performance under varying machine and experimental conditions. This investigation quickly evolved into a study of the performance of the secondary emission monitors as a function of beam energy, current, steering, foil surface conditions and target employed. Determination of the spatial variation of electron fluence involved the testing, calibration and employment of a new technique, that of radiachromic film dosimetry. The two investigations were conducted separately, although certain of the results of each were used in the analysis of the other.

II. FACTORS INFLUENCING THE PERFORMANCE OF SECONDARY EMISSION MONITORS

A. THE BEAM CURRENT MONITORING SYSTEM AT THE NPS LINAC

The beam current monitoring system currently in use at the NPS Linac consists of eight devices; four toroidal coils (hereafter referred to as "toroids"), two secondary emission monitors (hereafter referred to as "SEMS"), a zinc sulfide scintillating screen and a Faraday cup. These devices are deployed as shown in Figure 1.

A toroid is a toroidal coil of wire, wound around a doughnut shaped core of highly permeable material, usually ferrite. As the electron beam passes through the open center of the toroid, it induces a voltage in the windings which, ideally, is proportional to the beam current. The toroids at the NPS Linac are connected to an oscilloscope and present the machine operator with a visual picture of the electron pulse as it travels down the tube. Their susceptibility to radio frequency noise pickup and the fact that they produce no output current inhibits their use as precision monitors of total number of electrons; they remain qualitative, not quantitative devices. The use of toroids as precision monitors of integrated beam current is discussed in References 1-3.

The zinc sulfide screen fluoresces when struck by the electron beam. As the amount of light produced is a function of the beam flux, it offers a visual picture of the beam cross-section. This picture is presented to the machine operator by closed circuit television. It is used as the primary monitor of beam steering and focusing, as well as a crude but effective visual beam current monitor. Like the toroid, the zinc sulfide screen is a qualitative device. Unlike the toroid, it intercepts,

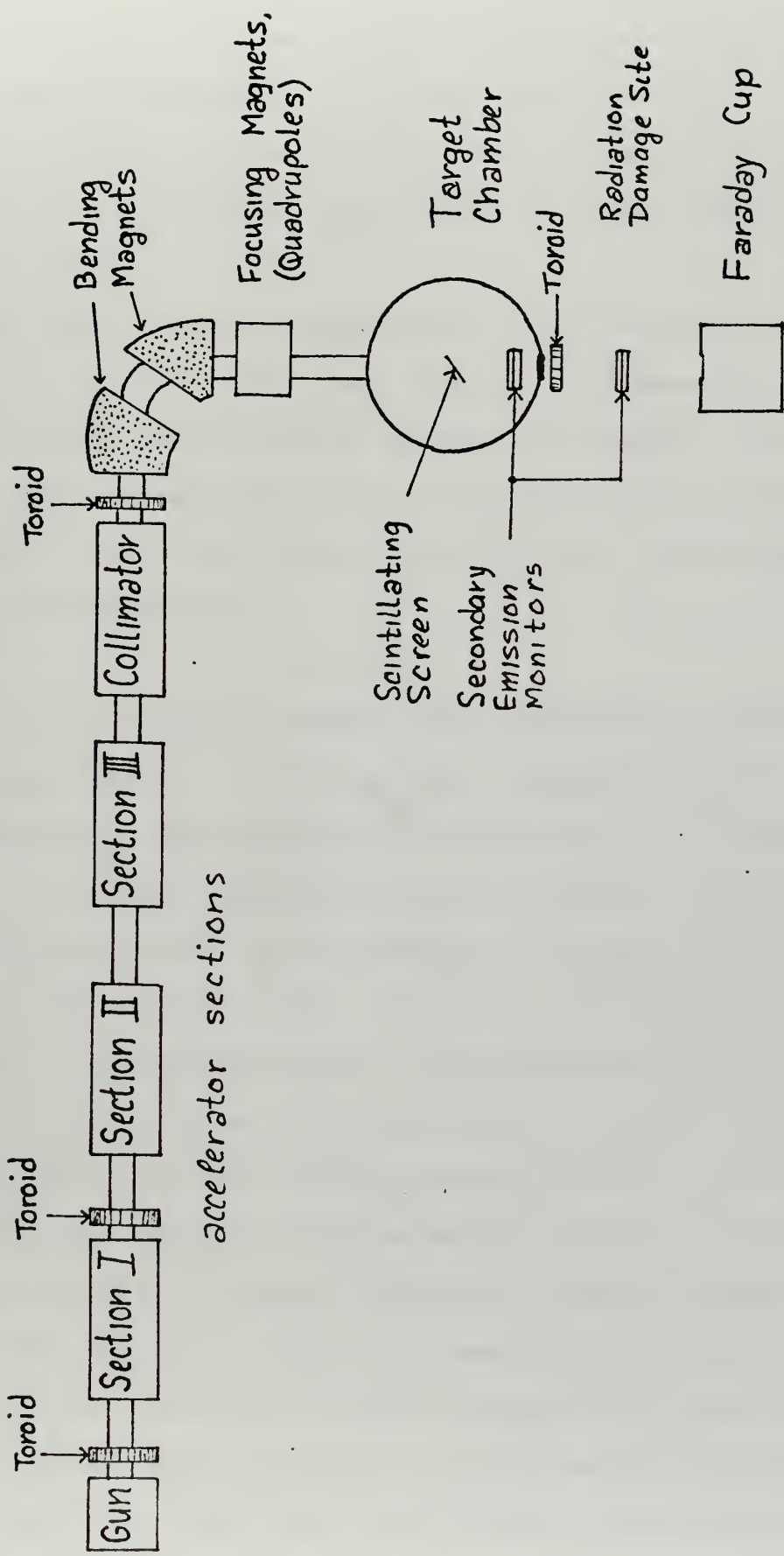


Figure 1. Schematic of NPS Linac Beam Current Monitoring System

and thus scatters, the beam and cannot be left in place during the performance of experiments. In reality, there is no single zinc sulfide screen; anything painted with zinc sulfide and placed in the beam will serve. For some radiation damage studies, the target itself is the zinc sulfide screen.

The Faraday cup stops the electrons in the beam, and their charge then charges a capacitor. The voltage developed on the capacitor is monitored by a vibrating reed electrometer and precision voltmeter. The charge collected equals the total number of electrons, if none are lost or introduced from sources other than the beam, and is easily computed using the relationship.

$$Q = CV$$

where Q is the charge in coulombs, C the capacitance in farads, and V the voltage in volts. The Faraday cup is designed to stop all of the electrons in the beam; in addition, it must stop all but a negligible amount of the electrons produced by shower formation. Since it stops and effectively counts all the electrons in the beam, it is the only absolute monitor in the system. It has two disadvantages, however. The process of stopping the electrons in the beam produces copious amounts of radiation which interferes with most precision experimentation. Also, it is located 75 cm from the target plane; hence some electrons are scattered when a target is in place and miss the entrance window of the Faraday cup (10 cm in diameter) and are not counted. For these reasons, the Faraday cup cannot be left in the beam during the experimentation in either nuclear scattering or radiation damage studies, hence cannot be used to measure the total number of electrons passing through the target. That measurement is performed by the secondary emission monitor.

B. DESCRIPTION AND THEORY OF OPERATION OF SECONDARY EMISSION MONITORS

A secondary emission monitor (SEM) consists of a series of thin metal foils, electrically isolated from each other, mounted with their plane surface normal to the beam. Alternate foils, designated emitter foils, are maintained at a moderately high negative DC potential. For the NPS Linac SEM's this potential is provided by a 250 volt battery pack. The remaining foils, designated collector foils, are connected to the virtual ground formed by a capacitor and vibrating reed electrometer. The outer foils are normally emitter foils; the field thus produced tends to repel low energy stray electrons such as might be produced by secondary emission in devices upstream from the SEM. The number of foils in a SEM reflects the desired sensitivity. In general, the more foils a SEM possesses, the higher its output current for a given beam current, and the more it will disturb and scatter the beam. The SEM's currently in use at the NPS Linac have three foils. Their general configuration is shown in Figure 2.

The electrons in the beam, in passing through the foils of the SEM, undergo electron-electron scattering, causing the surface to emit electrons much in the same manner as heat causing thermionic emission. These electrons are attracted to the positively charged collector foils and form a current which charges up the capacitor in exactly the same manner as previously described for the Faraday cup. For the three-foil SEMs at the NPS Linac, this current ranges from 2 to 4 percent of the Faraday cup current, or beam current.

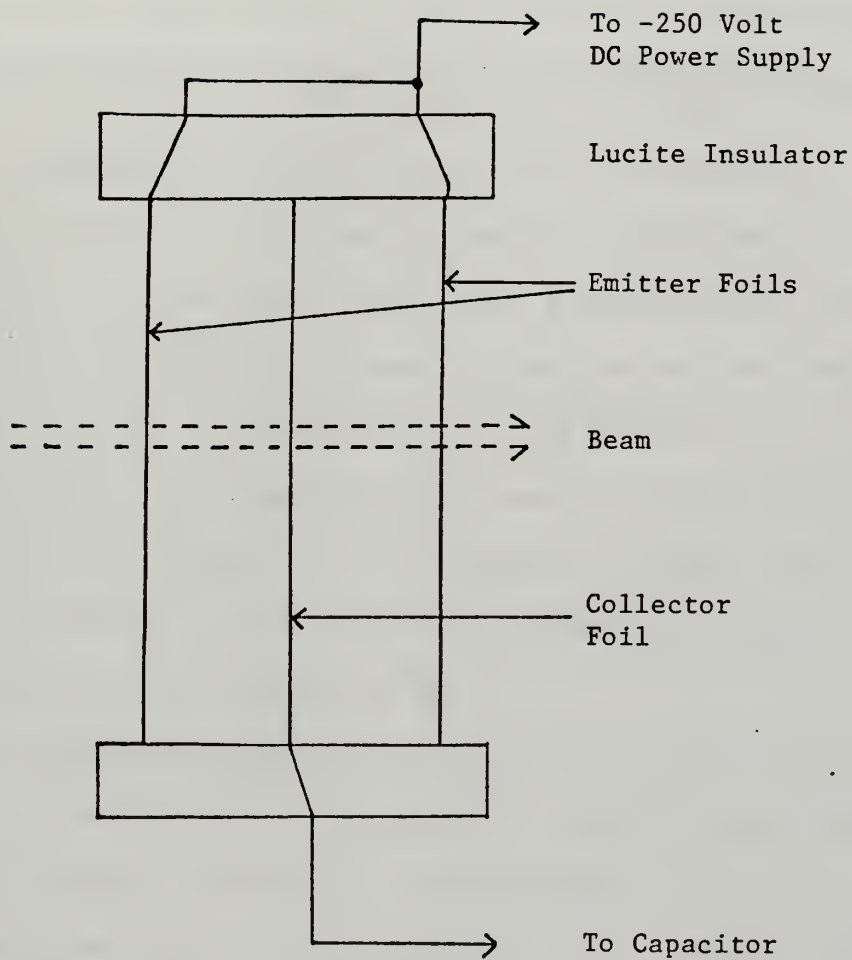


Figure 2. Construction of Sample Secondary Emission Monitor

The usefulness of the SEM depends on its minimal effect on the beam passing through it and the linearity of the relationship between SEM current and true beam current. A measure of this relationship is designated the "SEM Efficiency" and is expressed by the ratio:

$$\text{SEM Efficiency} = \frac{(\text{Charge collected by SEM capacitor})(100)}{(\text{Charge collected by Faraday cup capacitor})}$$

where the charges are produced by the same beam electrons. In practice, the SEM and Faraday cup are each connected to their own capacitor and electrometer, and the beam turned on for a given period of time. The voltages developed across each are measured and the charge ratio computed. It must be realized that the SEM Efficiency is not an absolute ratio, but is measured with respect to the Faraday cup. Fluctuations in efficiency can be produced by changes in the performance of either the SEM or the cup, and both possibilities must be considered before reaching any conclusions.

The study of SEM performance is really the study of the secondary emission process itself. A large body of work has been produced on secondary emission over the last three decades; some of the more prominent works are offered as References 4-7. An equally large body of work has been produced by the investigation of SEM Efficiency as a function of various parameters and conditions. Some of these works are listed as References 8-17. In general, however, there has been poor agreement between actual SEM performance as reported experimentally and theory, or even between experimentally derived conclusions drawn from data collected at different installations. Hence, the performance characteristics of an individual SEM cannot be accurately predicted from theory or empirical observations of other SEMs, but must be determined through actual experiment.

C. CONDUCT OF THE INVESTIGATION

The collection of data on SEM performance spanned a period of four months, from mid January to mid May 1972. In early May, a small explosion caused by overpressure in a hydrogen gas target destroyed the SEM which had been in use inside the target chamber for over a year. A new SEM, constructed identically to the older one, was installed and the experiments resumed. To an extent, this occurrence was fortunate, in that it not only allowed the correlation of results gathered on two different devices, but also permitted the observation of the effects of surface aging on SEM performance. Although the bulk of the data presented in this thesis was collected during the last few weeks of study using the newer SEM, sufficient data was taken on the older device to indicate that the conclusions reached were not special traits of one SEM, but general characteristics of similar devices as employed under the specific conditions at the NPS Linac.

The actual conduct of the experiment was simple. The accelerator was adjusted to produce a certain combination of beam energy, current, focusing or tuning. A target was selected if desired and placed in the beam. Other parameters, such as time or exposure to air, were introduced. Then, the SEM Efficiency was measured. Normally, five readings of the efficiency were taken at any one machine setting to allow for the averaging of statistical fluctuations. Typically, deviations of up to 0.5% occurred between individual readings, while the average efficiency determined by equivalent groups of readings would not differ by more than 0.1%, provided that the machine conditions for the groups were identical.

The selection of factors to test as possible influences of SEM Efficiency was accomplished by examination of the literature and by trial. Those factors which were specifically investigated include the surface condition of the SEM foils, the beam energy and current, the target or absence of target, and time.

D. SEM EFFICIENCY AS A FUNCTION OF FOIL SURFACE CONDITIONS

Of all the factors which influenced the SEM efficiency, the condition of the foil surfaces was the most dramatic. The surfaces were particularly sensitive to exposure to air and the electron beam. Periodically, the target chamber was returned to atmospheric pressure to permit repairs or changing of targets. This exposure to air invariably caused both a short and long term change in the SEM efficiency, with both changes being more pronounced with the newer SEM. Efficiencies measured as soon as possible after achieving the desired operating vacuum ($\sim 5 \times 10^{-6}$ mm Hg) were always found to be higher than the efficiencies measured prior to exposing the foils to air. During the ensuing 30 minutes or so, the efficiency would drift downward, eventually stabilizing at some point not in general the same as that prior to exposure. The fluctuations in individual SEM efficiency readings and hence in the average efficiency would continue higher than normal for several hours after regaining vacuum. An example of this recovery process is shown in Figure 3.

Repeated exposure to air, or perhaps just general aging of the surface brought on by continued exposure to the electron beam, led to a long term decline in SEM Efficiency. Just prior to the explosion, the older SEM exhibited a minimum efficiency of 2.61% which was achieved after a long period at sustained vacuum. The new SEM, with foils that had not been previously exposed to electrons, but did possess a normal coating of aluminum oxide, exhibited a normal efficiency of 3.27%.

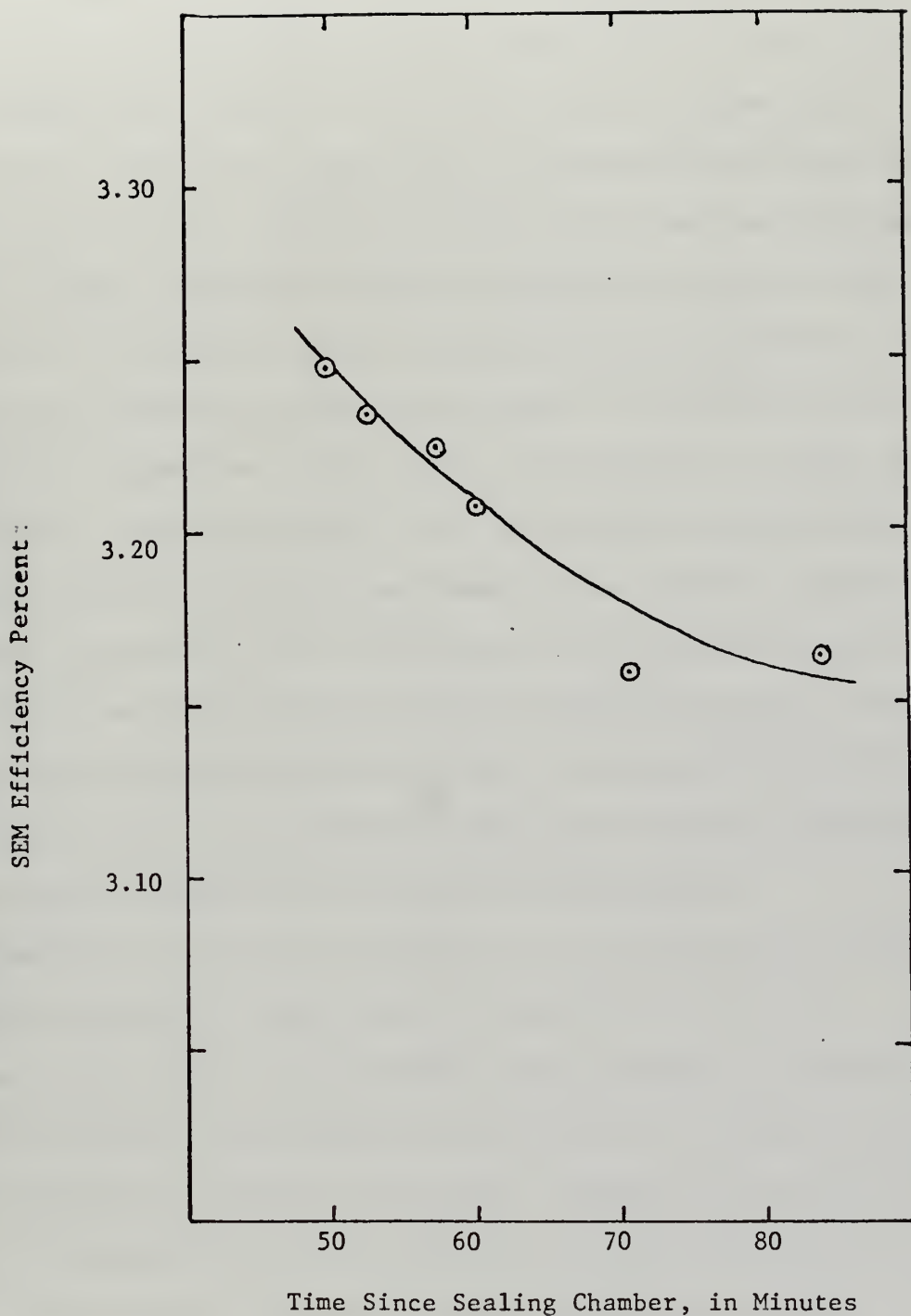


Figure 3. Variation of SEM Efficiency With Time Elapsed Since Exposure to Air

To investigate the possible effect of "fluence aging" on the surface, a series of efficiency readings were taken in which the beam was electromagnetically steered so as to pass through different areas of the foil surface. The initial effect was to increase the efficiency an amount ranging from 1 to 35%. Steering the beam could cause some electrons to miss the Faraday cup window, producing an apparent increase in SEM efficiency. It was found that moving the Faraday cup laterally a distance equal to the steering produced no such change in efficiency, hence the increase was assumed due to the surface characteristics. During the few minutes after steering the beam, after the initial increase in measured SEM efficiency, the efficiency was found to drop slightly, usually declining less than 2%. While there was little correlation between a particular area of the SEM foil and the resulting efficiency, the ensuing small drift downward was almost universal. The only spot which did not exhibit this behavior was that which represented the normal beam position, and was easily recognized by its dull brown appearance.

Apparently, the effect of exposure to the electron fluence was to decrease the ability of the surface to emit secondary electrons. Dell and Fotino [Ref. 10] investigated this phenomena at SLAC and found an increase in efficiency of about 2% over a 24 minute interval after initiation of exposure to the beam. Although this observation seems to directly contradict the experience here at NPS, it must be kept in mind that the situations at SLAC and NPS were different. It is quite possible that the much greater energy at SLAC coupled with the much larger beam size used in the experiment produced quite different effects.

E. SEM EFFICIENCY AS A FUNCTION OF BEAM ENERGY

Measurement of SEM efficiencies at several different beam energies ranging from 20 to 63 MeV were made. To reduce the influence of other factors, the measurements were made on the same day spaced as closely as possible in time. The series of measurements was performed four times, spanning a two month period and involving both old and new SEMs. In all cases, a general increase in efficiency with increasing energy was found, with the decrease being most pronounced at the energies approaching 20 MeV. The results of one of these series is presented in Figure 4; the results of the other three series were similar and only differed in the different baseline efficiencies observed on the particular day as a result of different surface conditions.

The observed increase in efficiency with increasing energy has been similarly observed by many other authors, [7, 10, 15, 17]. Vanhuyse and Van de Vijver [7] attribute this energy dependence to the effect of tertiary electrons ejected from the foil surface through interaction of the more energetic secondary electrons with the atomic electrons. The derived energy dependency is expressed by

$$Y(E, \xi) = G(\xi) + \alpha \ln(E)$$

where $Y(E, \xi)$ is the total yield of electrons, $G(\xi)$ is a function of foil thickness and α is a constant which considers the effect of material and surface conditions. The data presented in figure 4 were fit by linearized least squares regression to the above formula, producing the following expression for SEM Efficiency

$$\text{SEM Efficiency} = 2.215 + 0.141(\ln E)$$

As can be seen in Figure 4, the fit is good..

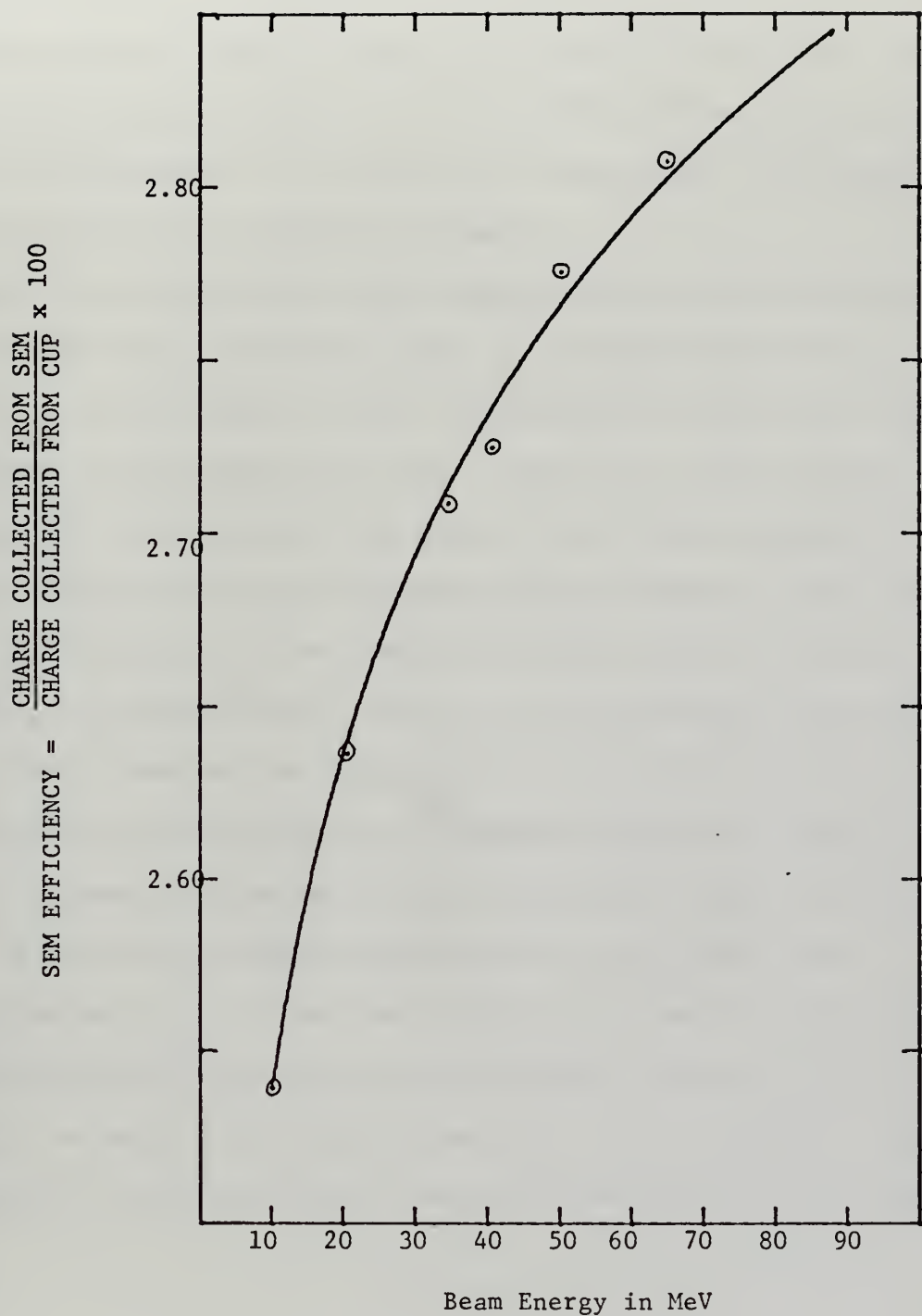


Figure 4. SEM Efficiency as a Function of Beam Energy

F. SEM EFFICIENCY AS A FUNCTION OF BEAM CURRENT.

Investigation of SEM Efficiency over a range of beam current from .04 to 0.5 μ a, at energies ranging from 20 to 55 MeV, failed to reveal any significant dependence of efficiency with beam current. The results of this investigation are presented in Figure 5.

It had long been observed that leakage currents were present in both the SEM and Faraday cup circuits; that is, charges would build up on both capacitors in the absence of beam. Investigations revealed that some of the leakage in the Faraday cup circuit, amounting to approximately 30 mv/minute, was produced by the action of the VacIon pump used to maintain vacuum in the cup. When this pump was turned off, the leakage stopped. The sources for the remaining leakage currents could not be found. It was determined, however, that these currents only appeared after initial beam had been established in the machine and could not be found when the machine had been completely shut down. Also, the currents appearing in the SEM and cup circuits were roughly in the same ratio as the SEM efficiencies resulting from actual beam current. These findings led to the conclusion that both currents are the result of residual acceleration of electrons emitted by the gun with no grid voltage. As such, they would not constitute a real leakage, but simply represented a low intensity beam produced by the machine in its standby mode.

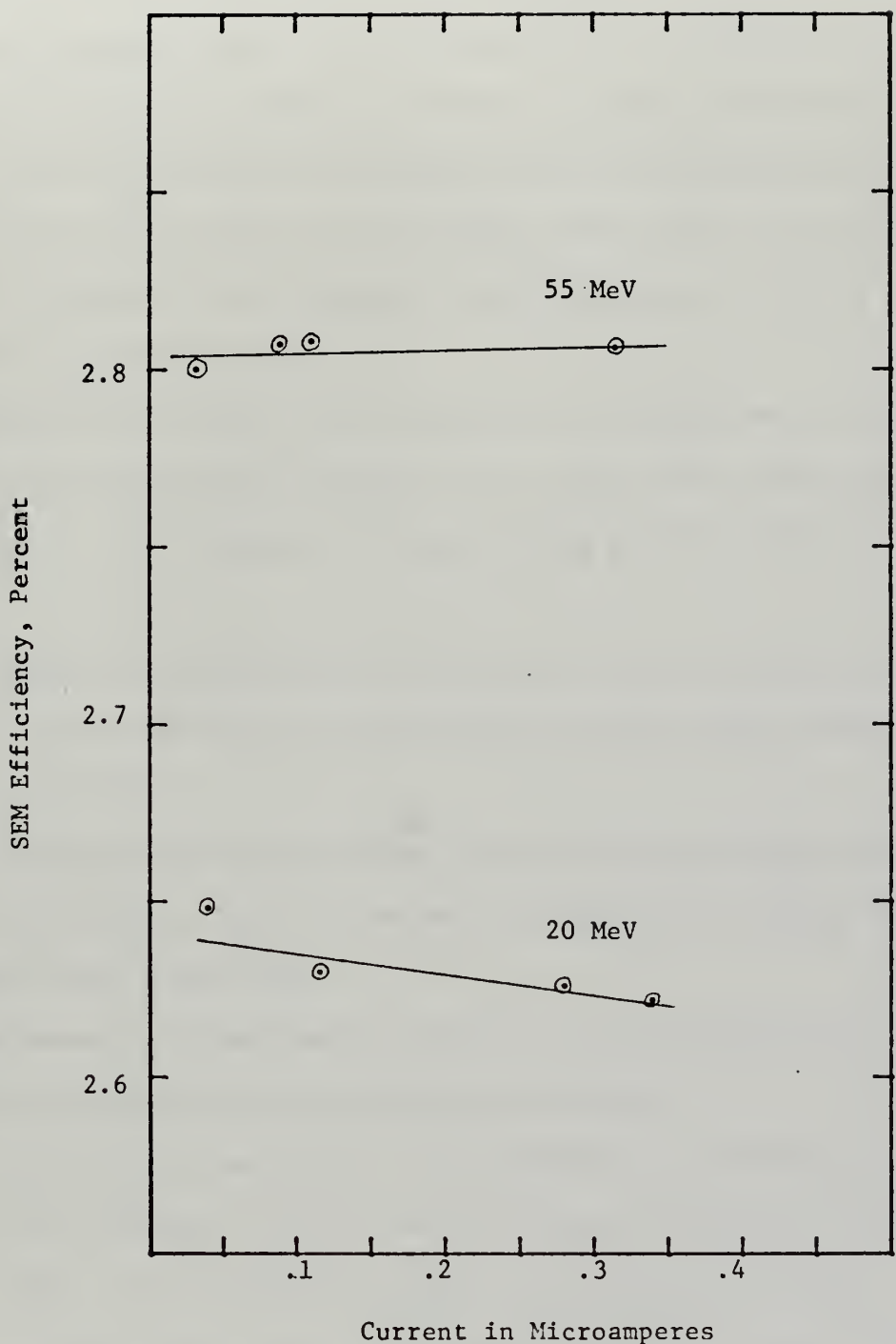


Figure 5. Variation of SEM Efficiency with Beam Current

G. SEM EFFICIENCY AS A FUNCTION OF SEM LOCATION

It has long been known at the NPS Linac that the introduction of any target into the beam causes an increase in measured SEM efficiency; in some cases this increase has exceeded 39%. The determination of the cause of this increase was of vital concern, since there was considerable debate as to whether SEM efficiencies should be measured with the target of interest in place or not.

Three possible causes for the increase in efficiency were considered:

1. Secondary electrons produced by the target were being caught by the SEM foils; or, if energetic enough, causing secondary emission in the foils.

2. Bremsstrahlung produced in the target in turn produces pair production in the SEM foils; the pairs then produce a double round of secondary emission.

3. Multiple scattering of primary electrons in the target causes a portion of the beam to miss the Faraday cup window while passing through the closer foils of the SEM.

All three causes were suggested by the fact that the SEM is much closer (20 cm) to the target than the Faraday cup (75 cm).

The first listed possibility is discredited by the observation that virtually all secondary electron emission produces electrons of energy 30 eV or less. The probability for high energy secondary electron emission is vanishingly small. This observation was not made at NPS but at other installations, as reported in References 4, 7 and 10. Since the outer foils of the SEM are maintained at a negative potential of 250 volts, no secondary electrons produced in the target can affect the SEM efficiency.

The second possibility is not so easily discredited. The problems of bremsstrahlung and pair production are not simply handled, and the energy ranges of interest at the NPS Linac unfortunately lie in a regime where no simple approximations can be used to provide reasonably accurate quantitative results. Heitler [18] presents a theoretical model which can be used to provide at least an order of magnitude estimate of the number of pairs produced in the SEM foils for a given electron fluence in the target. The assumptions and calculations using this model are presented in Appendix A. For a carbon target of thickness 40 mils, 3 SEM foils of 1-mil aluminum, and a beam energy of 20 MeV, the number of pairs produced was found to be on the order of 1.0×10^{-6} times the beam fluence. This number increased to 3×10^{-6} for a beam energy of 60 MeV. Thus the effect is far too small to account for the 35% increase in SEM efficiency observed. In addition, further investigation revealed that the largest increases in SEM efficiency resulted at the lowest energies; this is in direct conflict with the results predicted by the bremsstrahlung-pair production theory.

An estimate of the effect of scattering from thin targets is provided by Rossi [19]. An estimate of the root-mean-square angle of scattering for electrons is given by the expression:

$$\Theta_{rms} \approx \frac{E}{\beta E} (L)^{\frac{1}{2}} \approx \frac{21}{E} (L)^{\frac{1}{2}}$$

where $E = 2.1 \times 10^7$ eV, $\beta = v/c$, E is the electron energy in MeV, and L is the target thickness in radiation lengths. Using the same carbon target (40 mil) and ignoring the effect of scattering in the SEM foils or target chamber exit window, Θ_{rms} was calculated to be 6.9 degrees for 20 MeV, and 1.9 degrees for 60 MeV. Since the Faraday cup window is 75 cm away, these angles lead to a radial distance of

9.1 and 3.0 cm respectively. As the cup window is only 10 cm in diameter, the scattering could certainly lead to the observed increase in SEM efficiency. The effect of scattering in the foils and exit window, coupled with the defocusing of the beam as a function of distance from the center of the target chamber was investigated with radiachromic films as described in paragraph B-1, this thesis. Scattering angles of 0.8 degrees and 2.0 degrees were observed for 63 and 25 MeV respectively, with no target in place.

The increase in measured efficiency produced by the scattering of electrons by a target makes it imperative that actual efficiencies to be used in the conduct of experiments be measured with no target in place. The increase in efficiency produced by scattering is not real but only a result of the geometries of calibration. The actual efficiency, which is the ratio of the number of secondary electrons produced by the SEM to the number of primary electrons in the beam, will not change when the target is introduced.

III. INVESTIGATION OF THE LINAC BEAM PROFILE USING RADIACHROMIC FILMS

A. UTILIZATION AND CALIBRATION OF RADIACHROMIC FILM

1. Description of Film

Aminotriphenylmethane dye-cyanides of various types and configurations have been produced by the EG&G Corporation specifically for dosimetry in the megarad range. One of these materials, designated RACM-203, was selected for testing and possible use in determining the characteristics of the beam profile of the NPS Linac. RACM-203 is described by EG&G as a less than 1-mil thickness of a solid solution of hexahydroxyethylpararosaniline-cyanide in nylon on a 7 mil mylar substrate. Purchased in 6" by 8" sheets, the film was clear and transparent with one shiny and one dull side. The dull side was found to be the side bearing the dye. The mylar substrate proved to be quite stiff, a characteristic which made the film simple to emplace. The dye and nylon solution, however, proved to be rather soft, easily scratched and very soluble in alcohol. The film collected dust and fingerprints quite readily, and since both blemishes produced errors in reading the optical density, great care in handling was required. Handling and identification of individual film pieces was facilitated by attaching to each a small tag of transparent tape.

Humphreys and Wilcox [20, 21], researchers for EG&G, have reported that the films are linear in response over a dose range of 5×10^5 to 10^7 rads, with little or no energy dependence, no rate effects to over 10^{14} rad/sec, no fade during storage at room temperature, and no vacuum sensitivity. They are, however, sensitive to ultraviolet light. Exposure of a film piece to a four-tube ceiling fluorescent light

fixture at a distance of 2 feet for 48 hours caused an optical density change of .40, which corresponds to an exposure in the Linac beam of about 27 megarad.

2. Reading of Radiachromic Films

Films exposed to the electron beam exhibited a dull blue spot, which faded radially outward from the center. Some films developed a light pink spot center, indicating that a dose had been achieved that exceeded the limit of linear response. The general beam shape was quite evident from visual examination of the film, a fact which gave the film potential as a rapid diagnostic tool.

Reading the exposed film pieces consisted of determining the change in optical density as a function of location on the surface. For this effort, a photodensitometer was constructed which consisted of three main elements; a Unitron MEC3 binocular metallurgical microscope, an encapsulated photomultiplier tube with fibre optics probe, and a Gamma Model 2020 Photometer. The probe was inserted through a rubber cork which in turn was inserted into the right ocular of the microscope, the optics having been removed. Reading a film then consisted simply of moving the stage of the microscope the desired interval and reading the optical density on the photometer.

The films were designed to be read at a wavelength of 600nm. No adequate filter for this wavelength was available; however, one was found with response 590 ± 11 nm. Response curves offered by Humphreys and Wilcox indicate that such a range would be satisfactory. The filter was installed in the lamp housing of the microscope, and the beam spot narrowed to less than 1 mm by means of a diaphragm and lens. The size of the beam spot had no effect on the reading, but a small spot helped locate the portion of the target being examined more accurately.

A critical factor in the accuracy of film reading was the size of the microscope field of view. By changing objective lenses on the instrument, the diameter of the viewed area could be varied from 0.4 mm to 2.4 mm. Since the exposed areas on the films ranged from 1mm to 30mm in diameter, selection of the proper field of view was essential. Reading all films using the smallest field of view was undesirable, since the smaller the field of view, the more sensitive the response to dust particles, finger-prints, and imperfections in the film coating process. In general, beam spots less than 2mm in diameter as estimated visually were read with the 0.4mm objective, with readings taken every 0.1 mm. All the rest were read using an objective with field of view of 1.2 mm diameter, with readings taken every half or whole millimeter. Since in both cases the field of view exceeded the reading spacing, each reading represented an average optical density. Even so, it was found that on the smallest beam spots with the sharpest density gradients, movement of the microscope stage by less than a tenth of a millimeter produced density changes of more than .35, as read on the photometer.

Unexposed film possessed a residual optical density of .05 as compared to the empty microscope stage. Examined under the microscope, the film exhibited narrow banded striations oriented parallel to the sides of the film and spaced about 0.04 mm apart. The zero of the photometer was adjusted to a portion of the film which demonstrated a relatively constant optical density of .04-.06 over a reasonable area. It was not possible to zero the meter using the empty stage due to the impossibility of removing the film during the reading process without disturbing the relationship between film and calibrated stage. Since the photometer exhibited an annoying tendency to drift during operation,

rechecking of the zero every few readings was necessary; hence a spot on the film had to be used even if causing a slight chance for inaccuracy. Initially, of course, the "zero spot" was read with the meter zeroed to open stage to insure that the spot chosen did represent film that was unexposed, or so lightly exposed that no information could be obtained from it.

Normal reading procedure involved first locating the peak of the exposure pattern, then taking readings along both a horizontal and vertical section. For a few selected films, a complete two-dimensional array of density readings were taken, covering the entire film piece, or at least that portion which exhibited an optical density greater than 0.01. This latter procedure was used to investigate the symmetry or non-symmetry of the beam profile as well as obtain a graphical picture of the beam shape at selected points. It was quickly found, however, that for all points other than the target ladder, the profile was symmetrical enough to allow dispensing with the procedure and reverting to taking just two sections. Since the reading of an entire film piece took several hours, the reversion was welcome indeed.

3. Curve Fitting of Optical Density Readings

For convenient handling of data and interpretation, the optical density readings for each section across each film were fit to Gaussian curves of the form

$$OD = A \exp\left(-\frac{r^2}{\sigma^2}\right)$$

where OD is the optical density at the point r millimeters from the center of the profile. The parameters A and σ were obtained by linearizing the equation and performing a least squares regression using a programmable desk calculator.

It was quickly found that the regression procedure gave undue weight to the data points of lowest optical density. As a result, the curves produced fit the wings and sides of the profile well, but were up to 30% too low at the peak. By eliminating those points below .05 in optical density from consideration in the regression, new parameters were obtained that gave a much closer fit to all but those low data points. In most cases the abbreviated regression produced curves which fit the data well enough to suggest that the actual profile is very nearly Gaussian.

Figures 6 and 7 show examples of good and poor fits to Gaussian parameters. It should be noticed that even the poor fit is quite reasonable over most of the range of densities. The lowest readings are too high to fit the curve and their dispatch is rationalized on the grounds that they are too close to the background level of the film to be of great accuracy or significance.

The maximum optical density found on any film was 0.55. Doses corresponding to higher densities caused the film to solarize, that is to become light pink rather than dark blue. Films receiving too great a dose showed a Vesuvius profile, as depicted in Figure 8. Such profiles were of little use other than to show the general beam shape. They could not be fitted to Gaussian parameters, since not only was the location of the profile center unknown, but the number of valid data points was limited. The first problem was most serious, since the first step in the reading procedure is to locate the center of the profile. The issue, of course, is of no practical consequence; one need only limit the fluence to a range which produces no polarization.

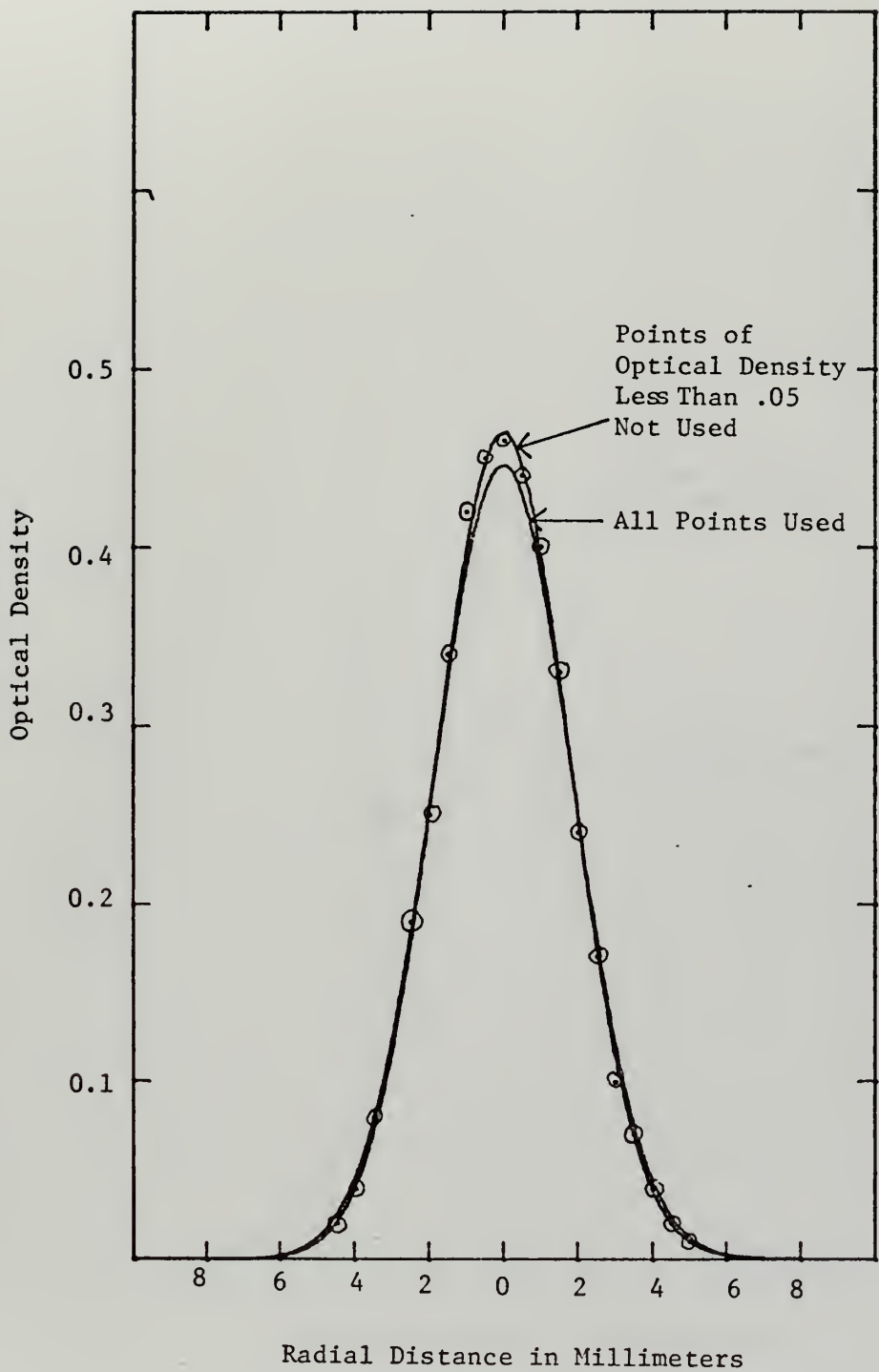


Figure 6. Example of Good Fit of Beam Profile to Gaussian

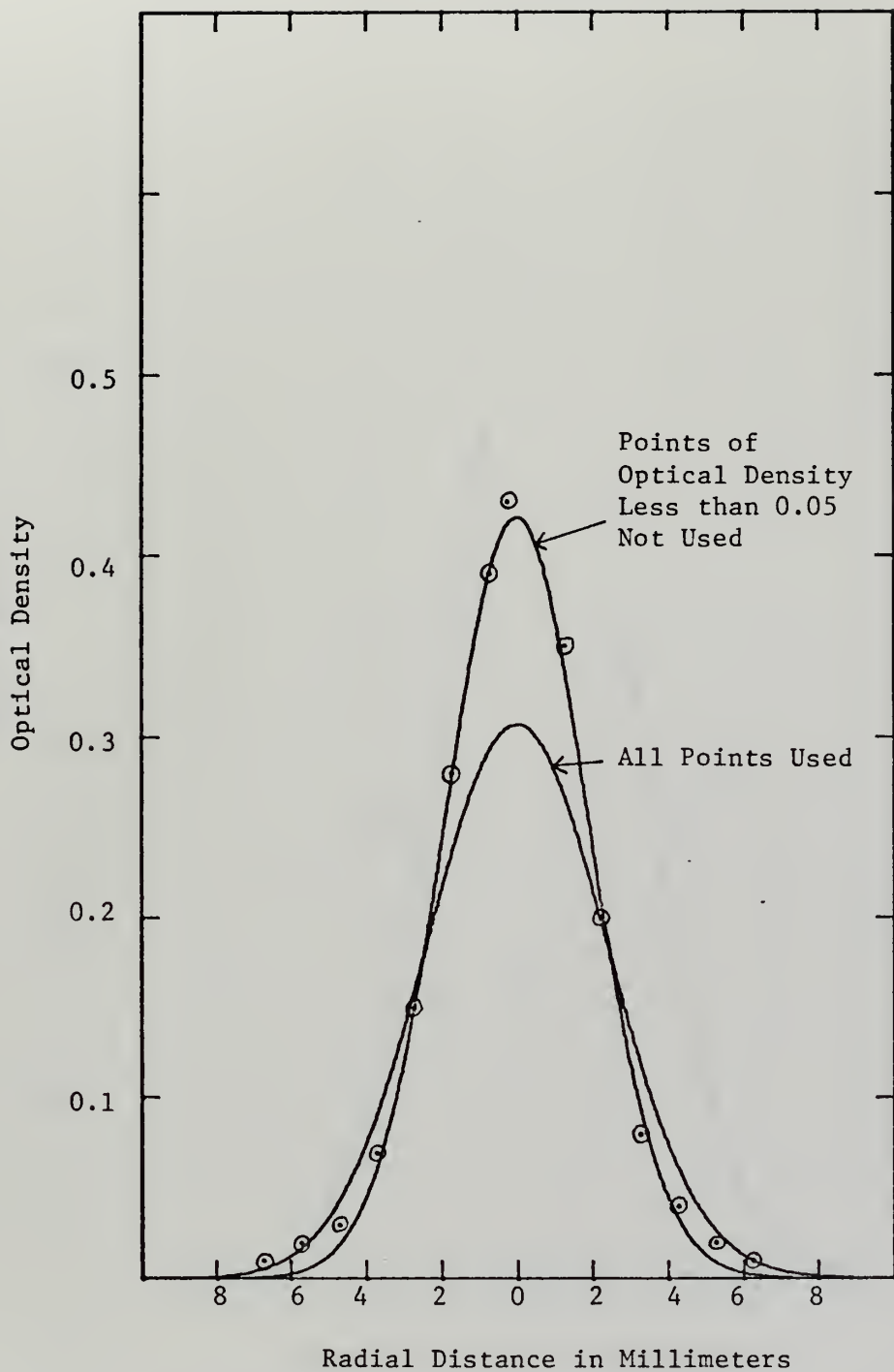


Figure 7. Example of Poor Fit of Beam Profile to Gaussian

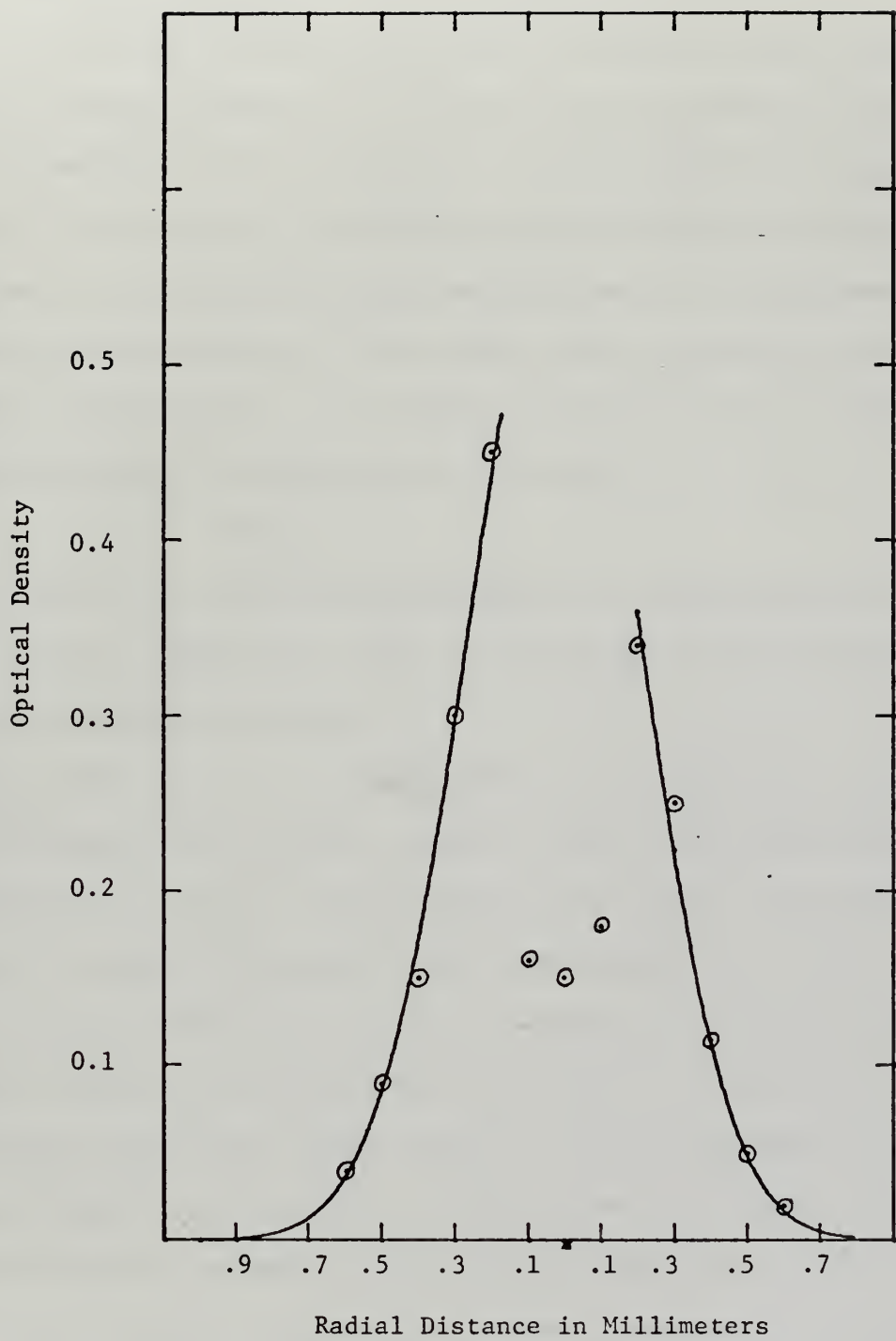


Figure 8. Example of Non-Linear Film Response

4. Calibration of Films

Film calibration consisted of the determination of the relationship between absorbed dose and the resulting change in optical density. This was accomplished using the linear accelerator itself. The total number of electrons causing each film profile was measured using the Faraday cup or a calibrated secondary emission monitor. This number of electrons was then correlated to the volume under the surface formed by the optical density profile. This volume, expressed in terms of the Gaussian parameters, is represented by the formula

$$V = \pi \sigma_h \sigma_v A$$

where σ_h and σ_v are the deviation parameters for the horizontal and vertical sections respectively, and A is the average of the horizontal and vertical amplitude parameters.

If the optical density is proportional to dose, which for a given energy is proportional to fluence, then the volume determined above should be proportional to the total number of electrons causing the exposure. The ratio n/V should be the same for all films exposed at a given energy. As can be seen from the table in Appendix B, this is not quite true. The computed ratio ranges from 1.36×10^{15} to 4.69×10^{15} . However, if the values obtained from films exposed at the target ladder and Faraday cup window are discarded, and they certainly represent poor fits to the Gaussian parameters, the remaining films show a ratio which is remarkably constant considering the relative crudeness of the procedure. This ratio has an average value of

$$(2.00 \pm .07) \times 10^{15}, \text{ for 63 MeV.}$$

The correlation of optical density with electron fluence at 63 MeV may be made. The ratio n/V represents the constant of proportionality between density and fluence:

$$F = \frac{D}{V} OD = (2.0 \times 10^{15}) OD \text{ electrons/cm}^2$$

where OD is the optical density produced by the fluence F. at a specific point.

The relationship between fluence and absorbed dose is expressed as:

$$D = K(E) \cdot F$$

where $K(E)$, the dose conversion factor is given by the expression

$$K(E) = 1.6 \times 10^{-8} \frac{dE}{d\xi}$$

where $\frac{dE}{d\xi}$ is the collision stopping power, defined as the average energy loss due to collisions per unit path length, length being expressed in gm/cm^2 .

Berger and Seltzer [Ref. 25] have compiled an extensive tabulation of values of collision stopping power for various materials over wide ranges of electron energy. This listing does not include mylar, but does include polyethylene. Since mylar is a derivative of polyethylene with similar chemical structure, [25] and since the values of collision stopping power for all plastics considered by Berger and Seltzer do not differ by more than 8% from each other, the collision stopping power for polyethylene was used to calibrate the radiachromic films.

Figure 9 shows the collision stopping power and dose conversion factor as functions of beam energy. Absorbed dose data may be computed from optical density data by sing the relationship

$$D = K(E) F = KA (2.0 \times 10^{15}) \text{ rads}$$

The relationships between optical density and dose for 25 Mev and 63 Mev are presented in Figure 10. Of significance is the observation that the effect of energy is rather slight. Since the effective range of usable optical density is .05 to .55, the usable dose range of the film is about 5-40 megarads.

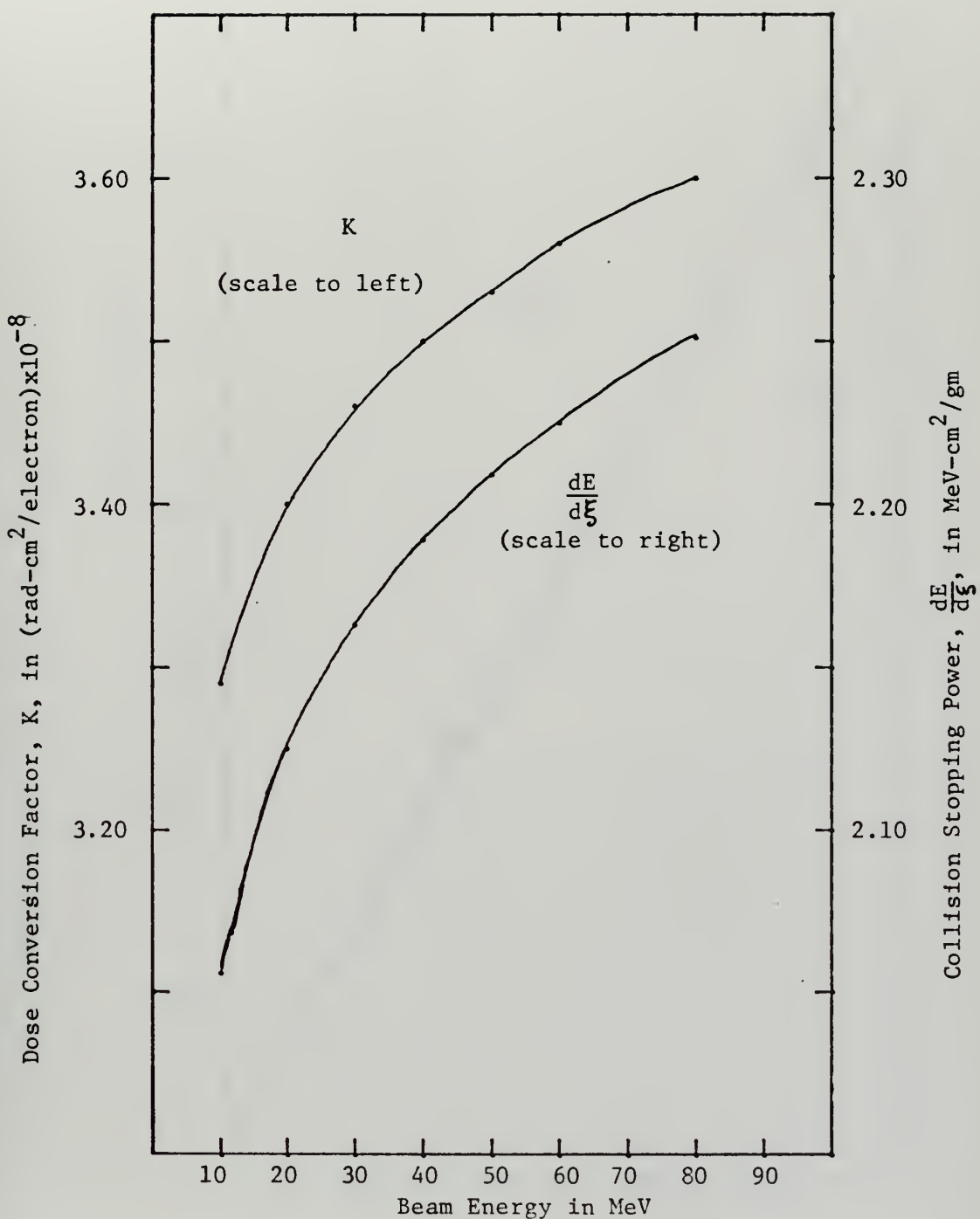


Figure 9. Collision Stopping Power, $\frac{dE}{d\xi}$ and Dose Conversion Factor, K , for Polyethelyne as Functions of Beam Energy.

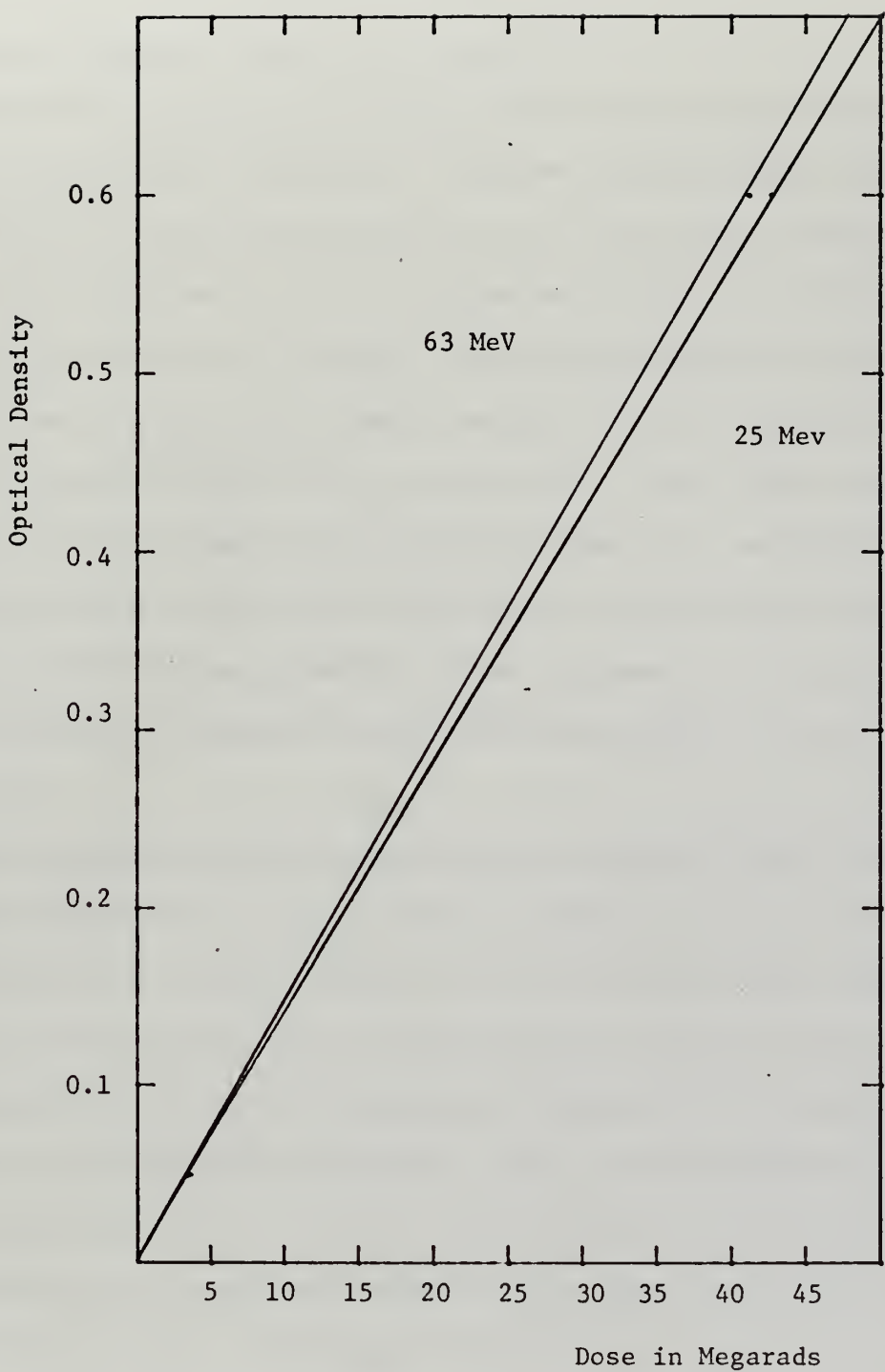


Figure 10. Relationship Between Absorbed Dose and Radiachromic Film Optical Density

B. INVESTIGATION OF THE LINAC BEAM PROFILE

1. Beam Profile as a Function of Location

The general configuration of the beam profile was that of two Gaussians intersecting at the center. The beam spot so produced tended to be elliptical. This shape was expected, since for proper resolution of the magnetic spectrometer the quadrupoles were set so as to produce a spot that is wider than it is high. The elliptical shape was quickly degraded by scattering in the secondary emission monitor and exit window and the fact that the beam was only focused at the target ladder position. As a result, the beam shapes at the radiation damage site and Faraday cup window were more circular than elliptical. This observation is reflected in the deviation parameters listed in Appendix A; as can be seen, the differences between the horizontal and vertical sections were not great.

The beam shape at the target ladder at 63 MeV was nicely elliptical, with a width roughly twice as great as its height. The shape at 25 MeV was not elliptical but quite distorted. As seen in Figure 11, a flare developed on some profiles, while others assumed a triangular shape. This deviation from the expected ellipse was apparently due to improper adjustment of the quadrupoles themselves. Even with this distortion at the target position, however, the exit window films at 25 MeV exhibited a quite good elliptical shape, and the films at the more distant positions were generally circular. (See Figures 12-17)

The profiles at the target position could not, in general, be fitted to Gaussian parameters, as the shape was not symmetrical. Figure 13 shows the general beam profiles at the target ladder for the two energies. For both, the profile is seen to have a smaller deviation

to the right than to the left, as viewed facing the incoming beam. Again, adjustment of the quadrupoles must be tagged as the culprit. The deviation from symmetry is not significant for operation of the accelerator, but does render somewhat invalid the computation of Volume as discussed in the section on calibration.

Scattering of the beam and divergence of the focusing caused the profiles to increase in size as the distance from the target ladder increased. Figures 18-19 depicts the beam profiles for the three external positions, normalized so that each profile represents the same exposure. The attenuation and spreading out of the beam is somewhat more pronounced at 25 Mev. Using σ as an indicator of beam spreading, a plot of spreading versus distance from the target ladder was made. As shown in Figure 20, the angle of dispersion was quite different for the regions inside the target chamber and outside. It is thought that the slight angle between target and exit window results primarily from the defocusing action of the quadrupoles at locations other than the focus plane, while the larger angle between exit window and Faraday cup results from the defocusing plus the effect of scattering in the secondary emission monitor and exit window. It is noticed that the defocusing at 25 MeV is slightly greater than at 63 MeV, while the scattering is roughly twice as large.

2. Beam Profiles as a Function of Absorber

To investigate the effect of cascade showers in thick absorbers, films were placed before and after absorbers arranged in stacks. The absorber materials used were Beryllium and lead. A single thickness was exposed at 25 MeV, while at 63 MeV, 4 thicknesses of lead and 8

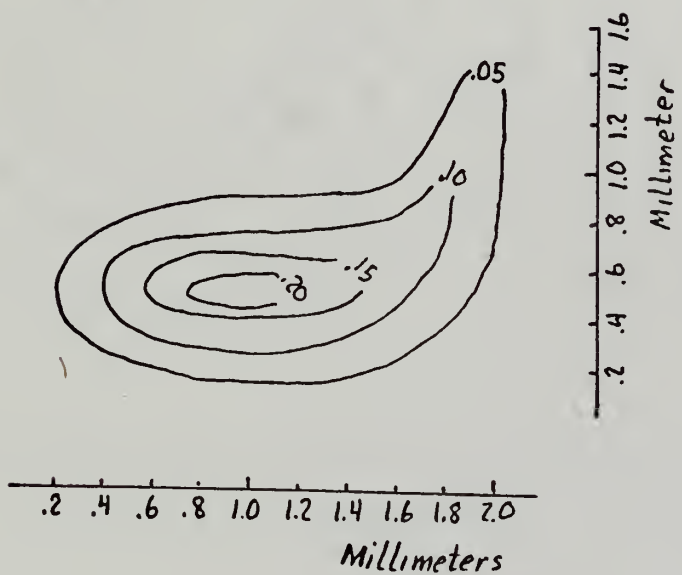
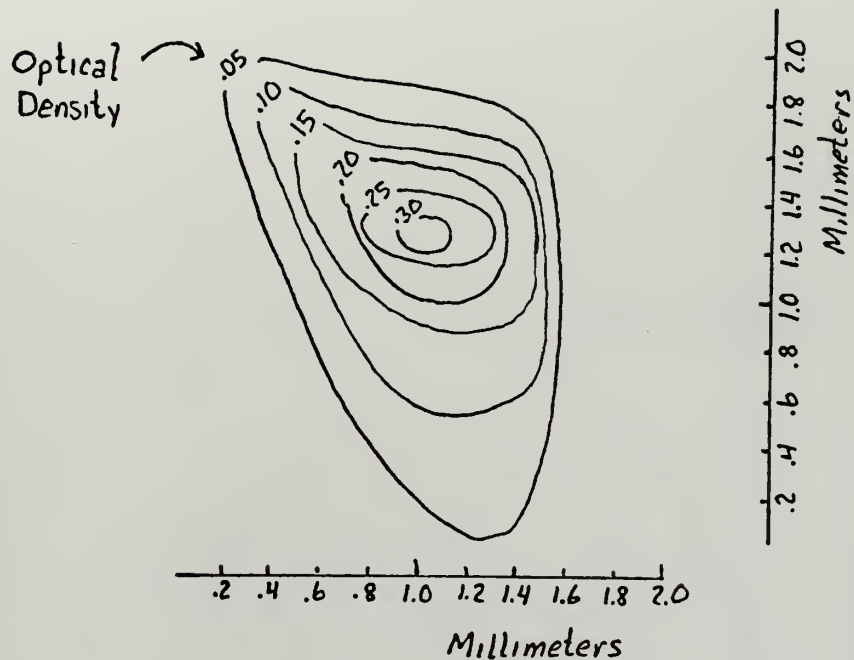


Figure 11. Representative Beam Profiles at Target Ladder, 25 MeV, Showing Distortions of Expected Elliptical Shape

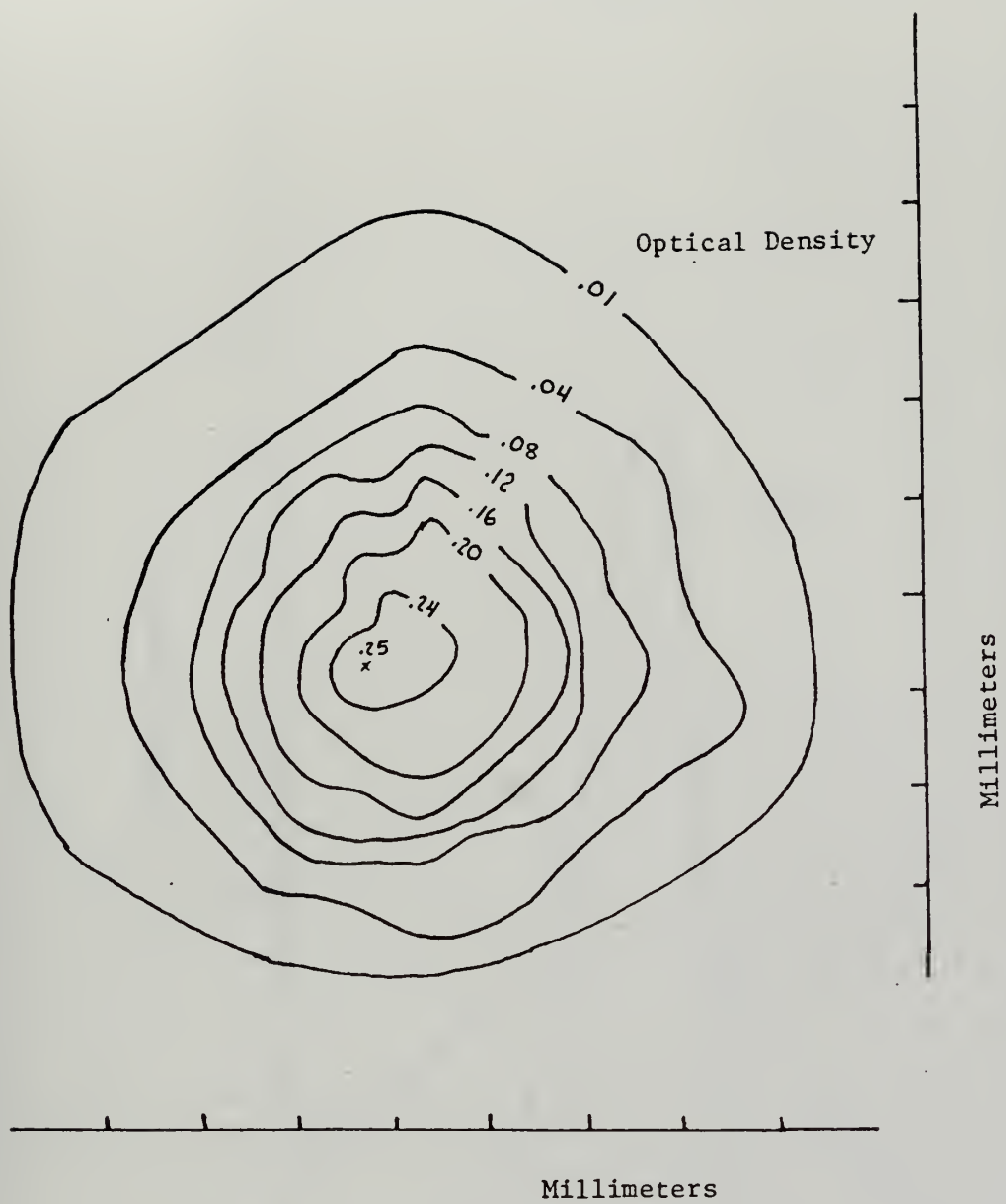


Figure 12. Representative Beam Profile at Radiation Damage Site, 63 MeV

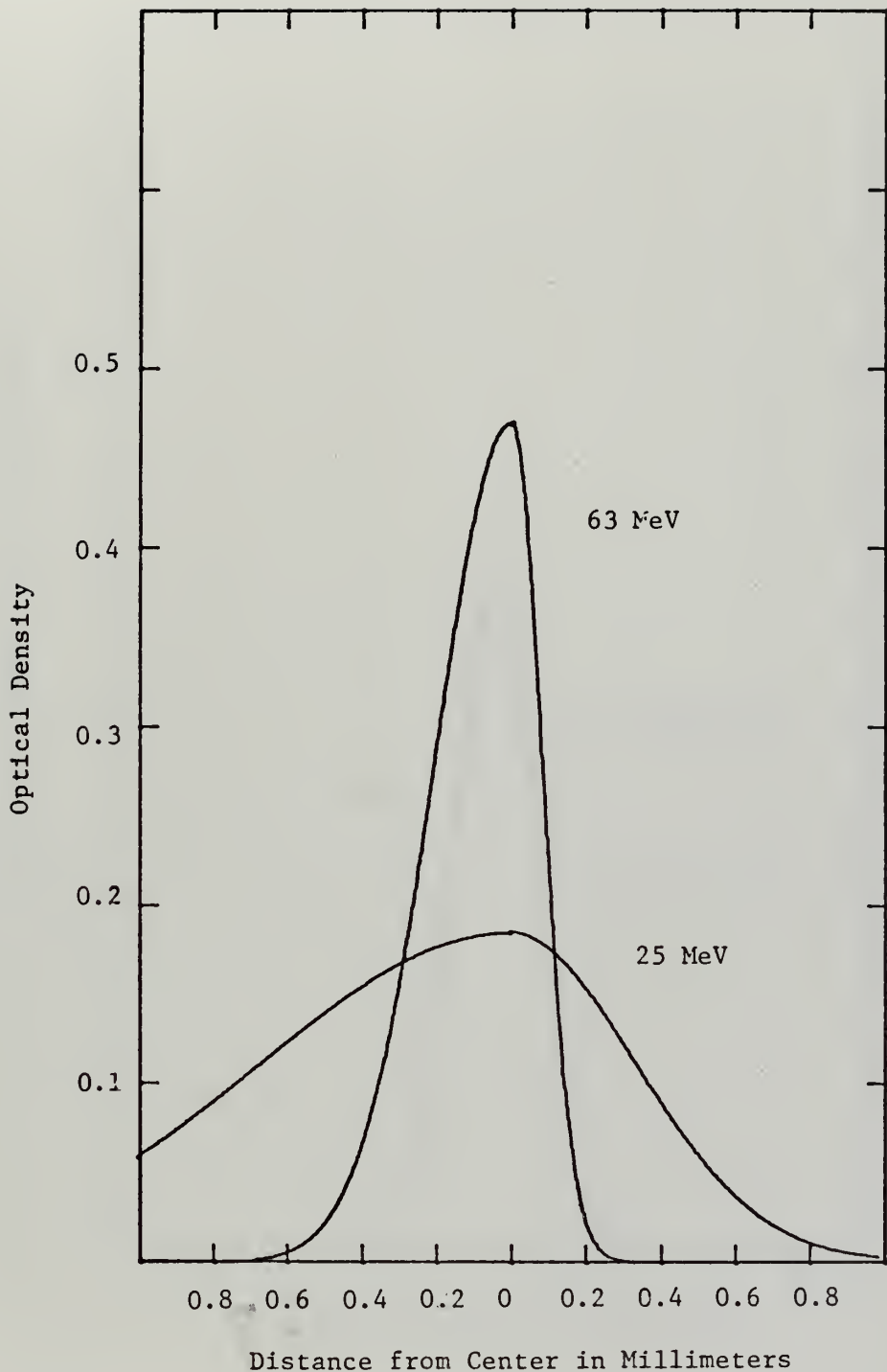


Figure 13. Non-symmetry of Target Ladder Beam Profiles.
(Horizontal Section)

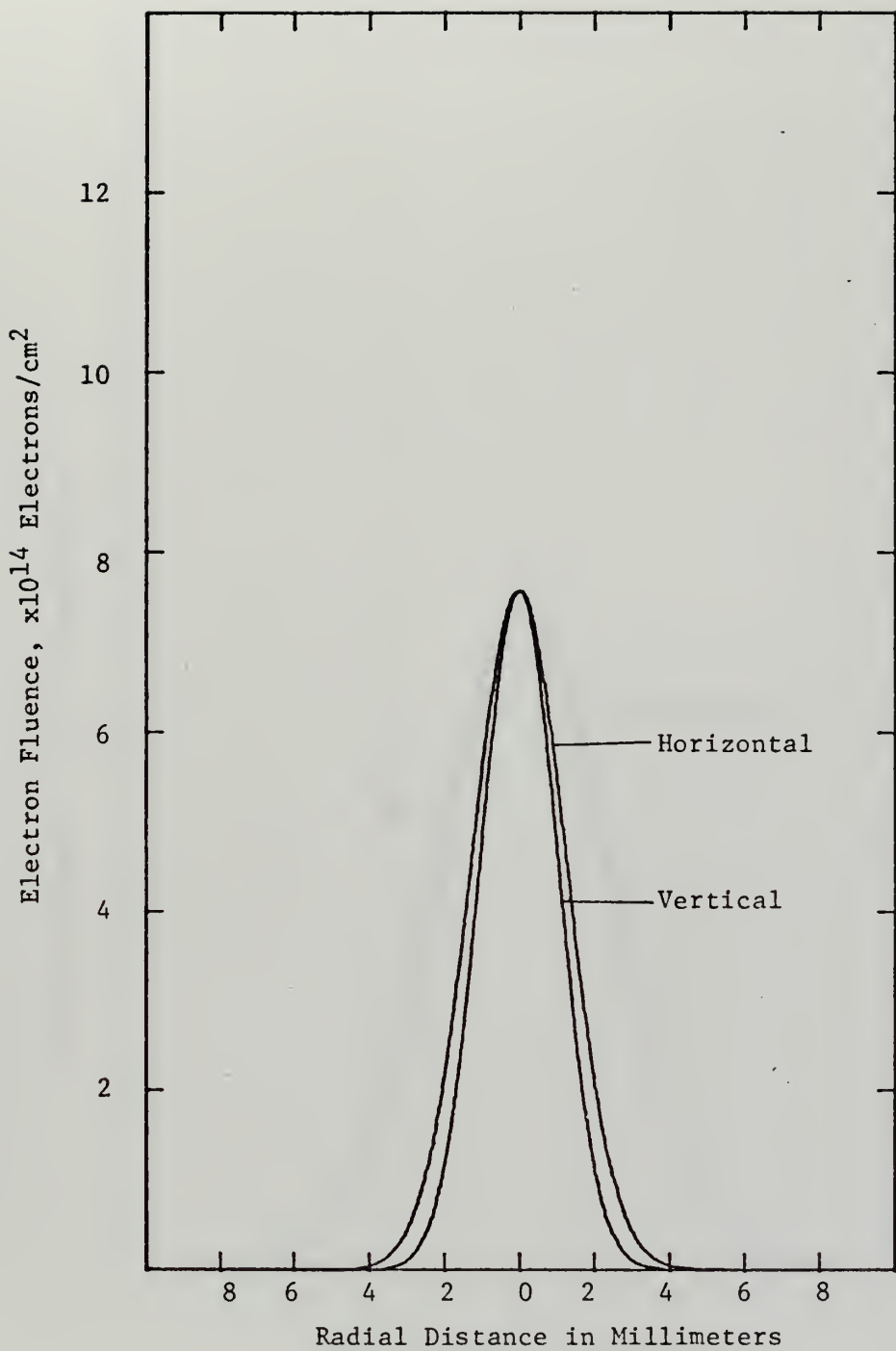


Figure 14. Example of Non-Isotropy of Beam Profile, Exit Window, 63 MeV

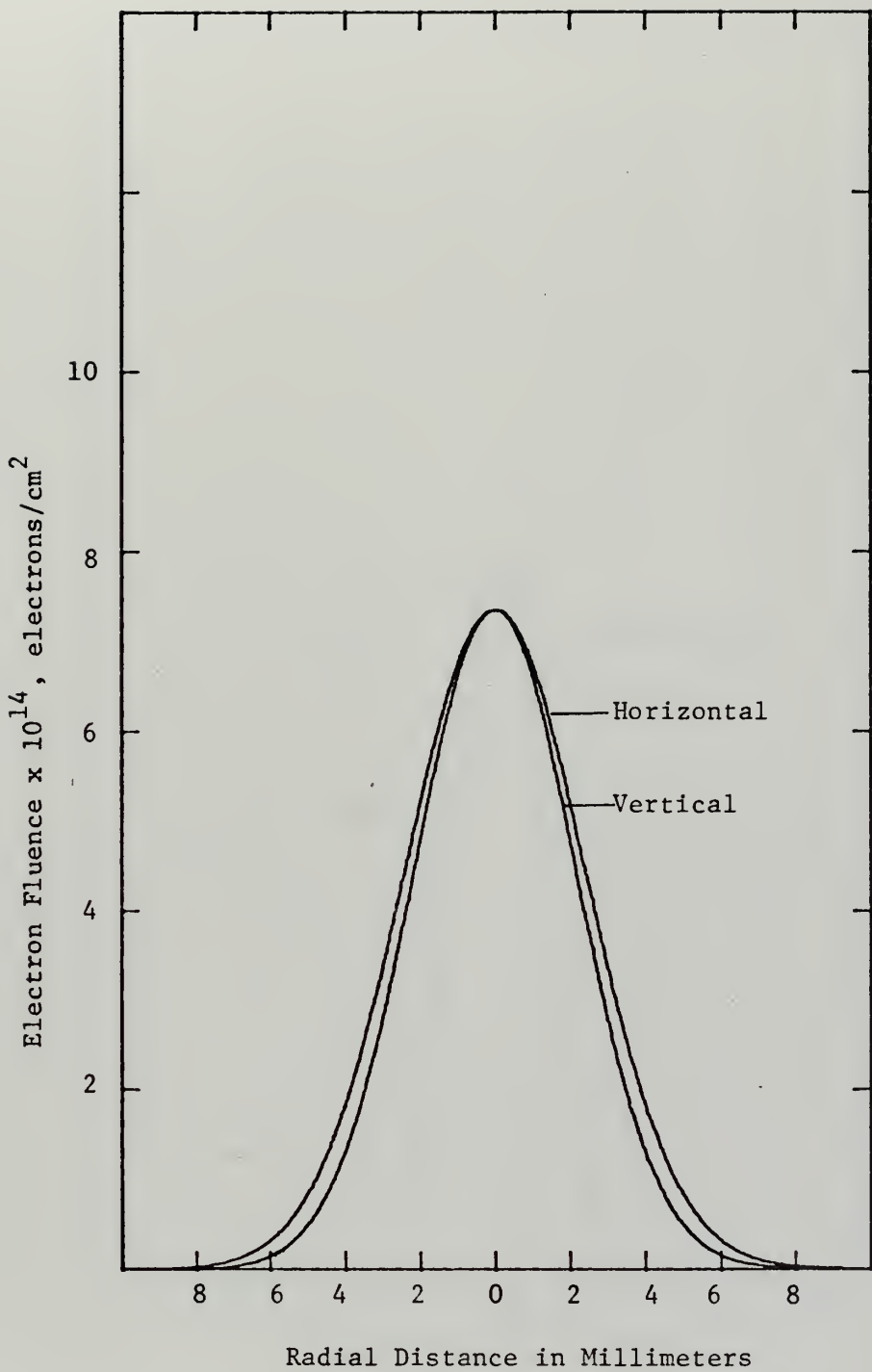


Figure 15. Example of Non-isotropy of Beam Profile, Radiation Damage Site, 63 MeV

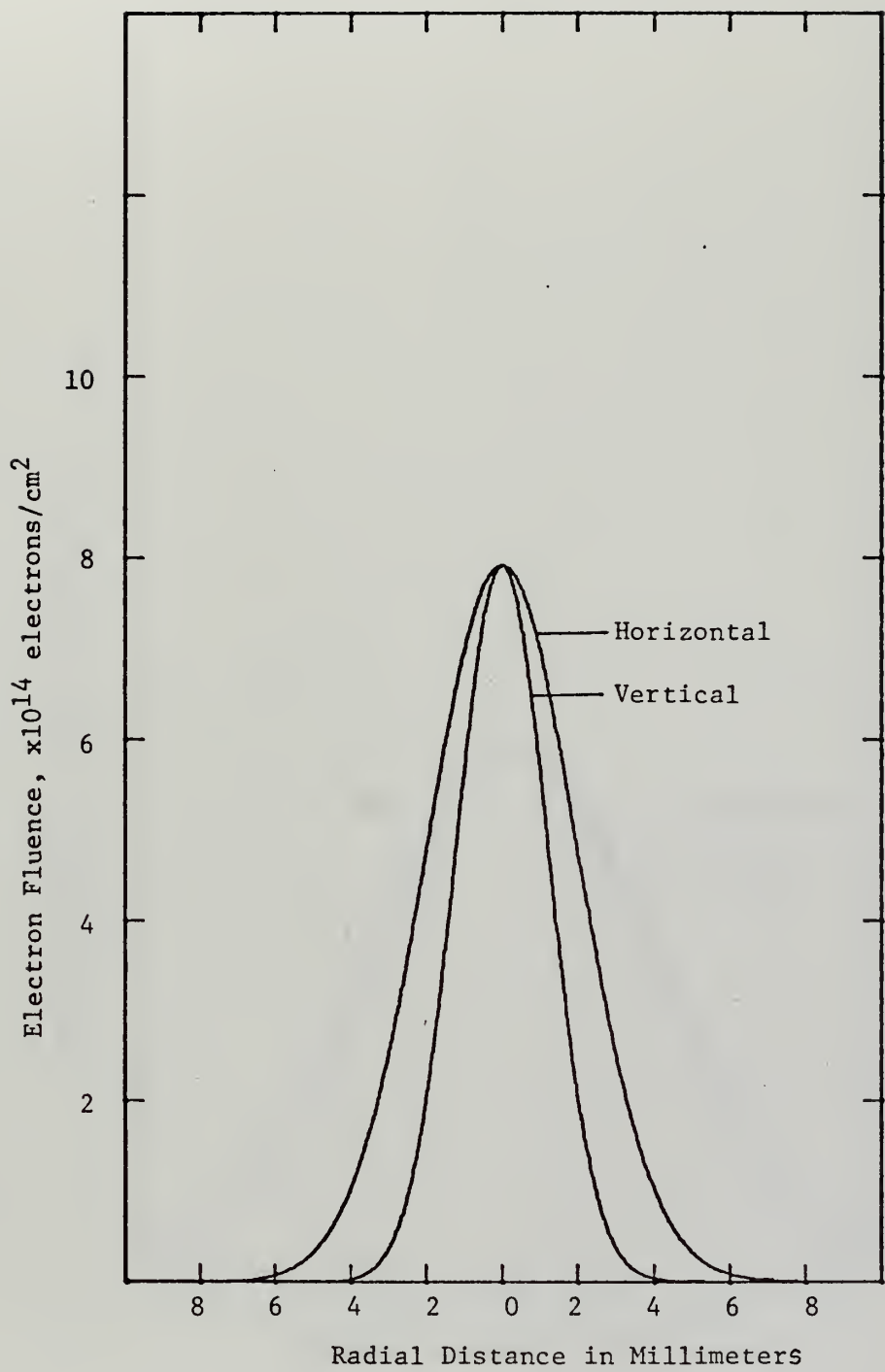


Figure 16. Example of Non-isotropy of Beam Profile Exit Window, 25 MeV

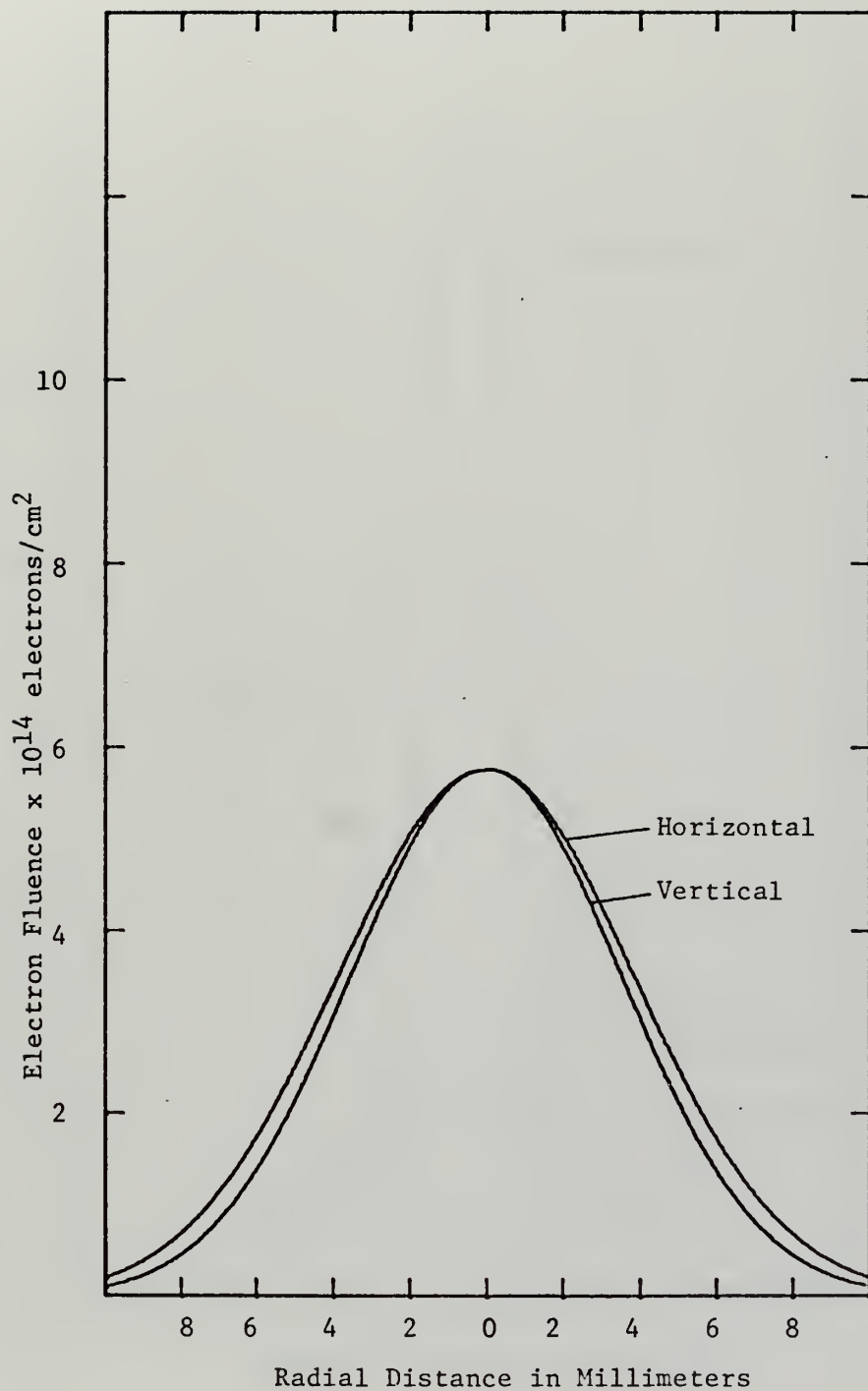


Figure 17. Example of Non-isotropy of Beam Profile Radiation Damage Site, 25 MeV

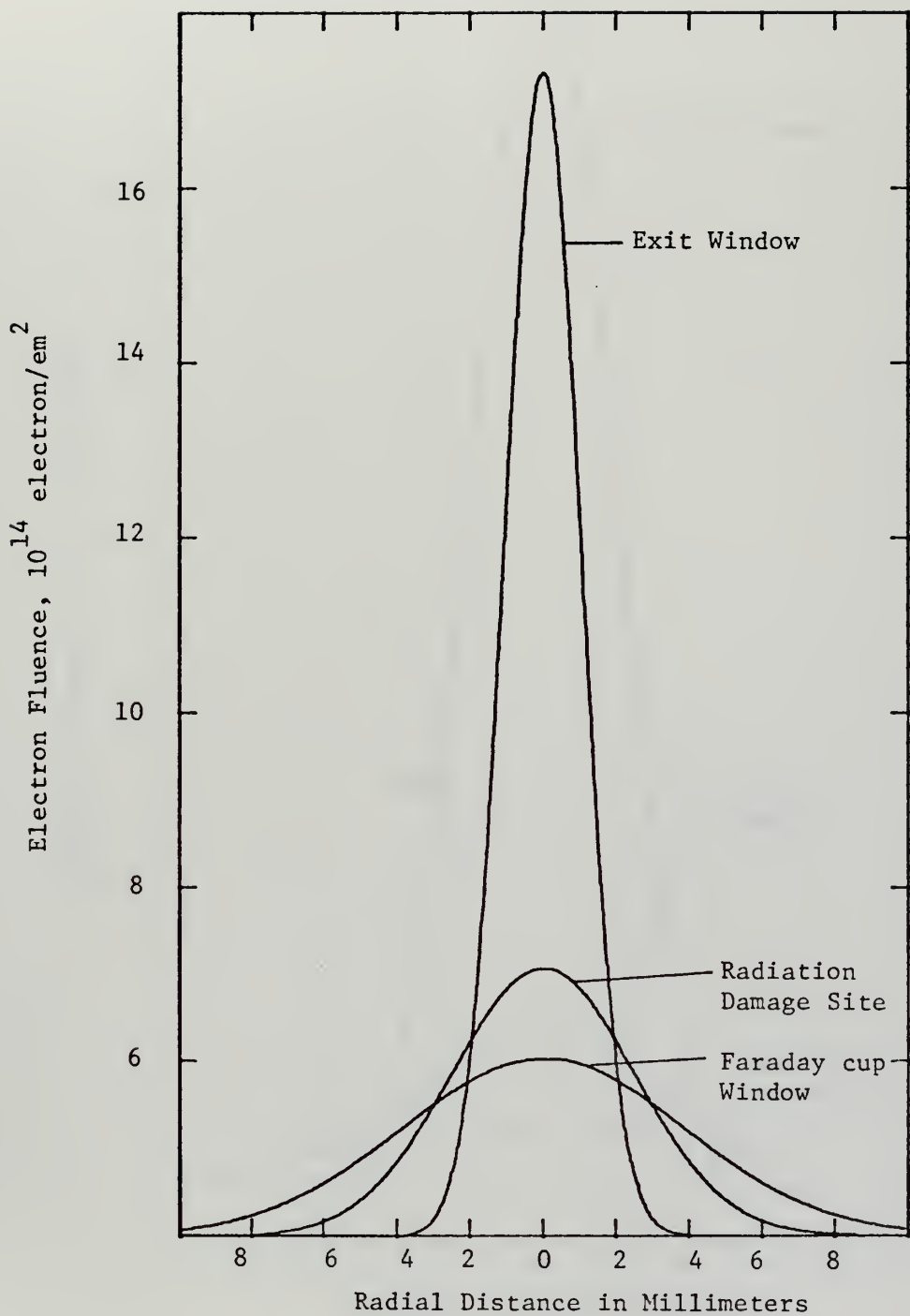


Figure 18. Comparison of Beam Profiles at Three Sites Outside Target Chamber, 63 MeV

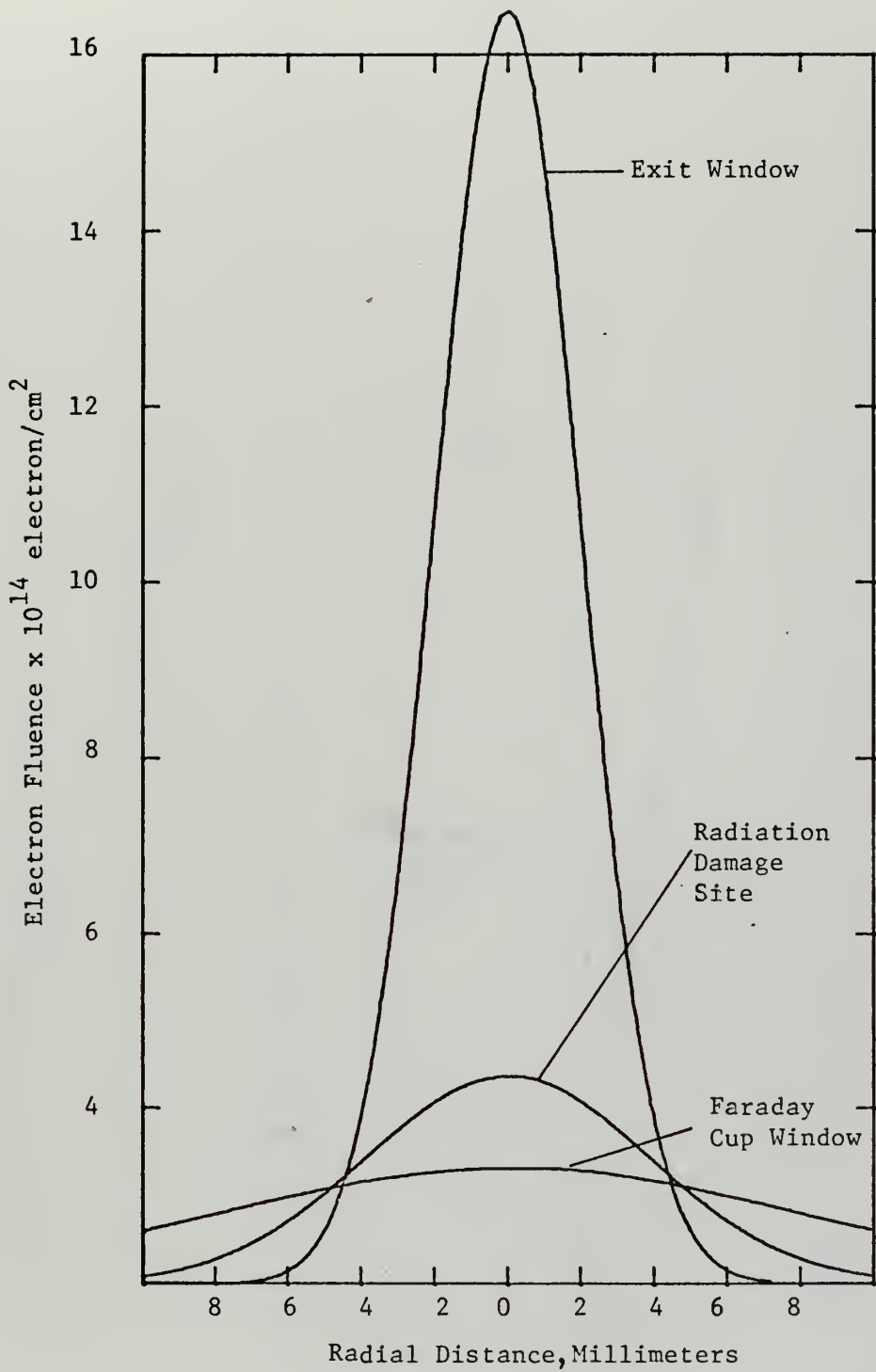


Figure 19. Comparison of Beam Profiles at Three Sites Outside Target Chamber 25 MeV

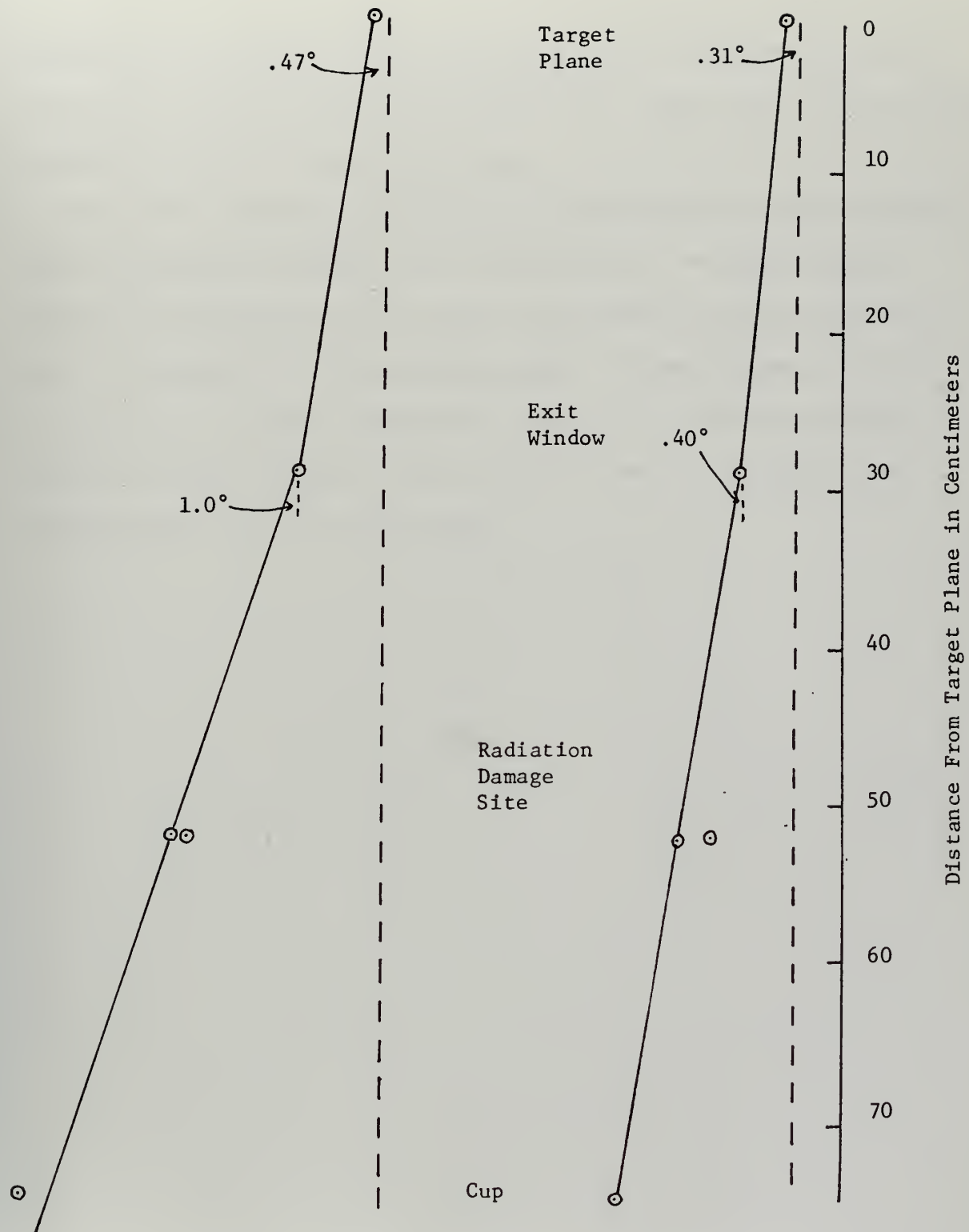


Figure 20. Angular Dispersion of Beam Past Target Plane. Points Represent values of σ from Gaussian Curve Fitting. Points at Radiation Damage Site Reflect Maximum and Minimum Values.

thicknesses of beryllium were used, giving a total thickness in lead of 1.32 cm, (15.0 gm/cm^2) and 3.25 cm (5.9 gm/cm^2) of beryllium. The resulting profiles are shown in figures 21 to 24.

The effect of showers is indicated by computing the volumes resulting from the Gaussian parameters fit to the profiles. As these volumes should be proportional to the fluences, they should reflect the size and spatial distribution of the resulting shower. These volumes are plotted as functions of absorber thickness in Figure 25. In lead, the shower buildup is clearly evident; this is not the case for beryllium, since the thickness in gm/cm^2 is much less.

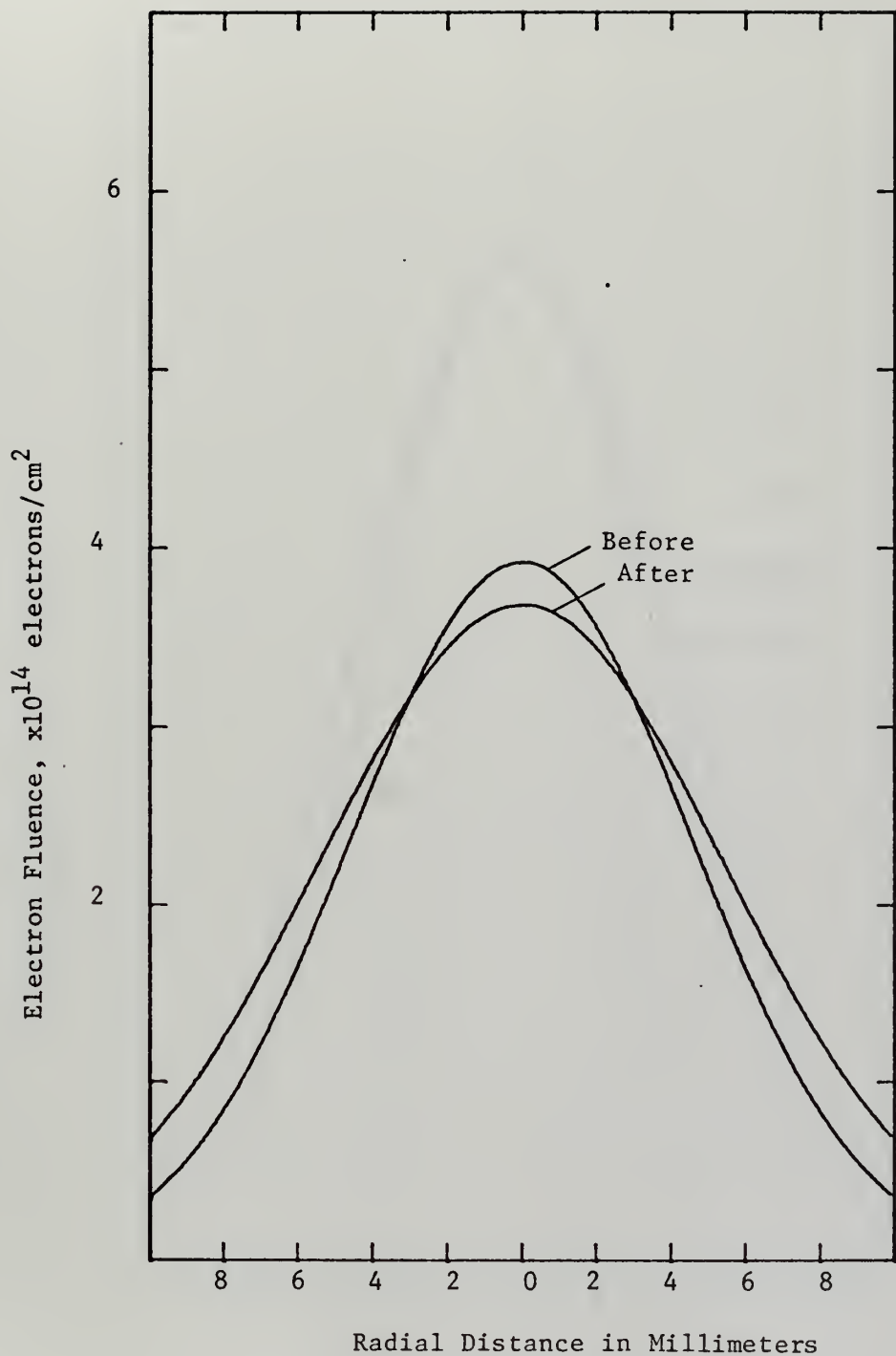


Figure 21. Beam Profile Before and After Lead Slab, 25 MeV

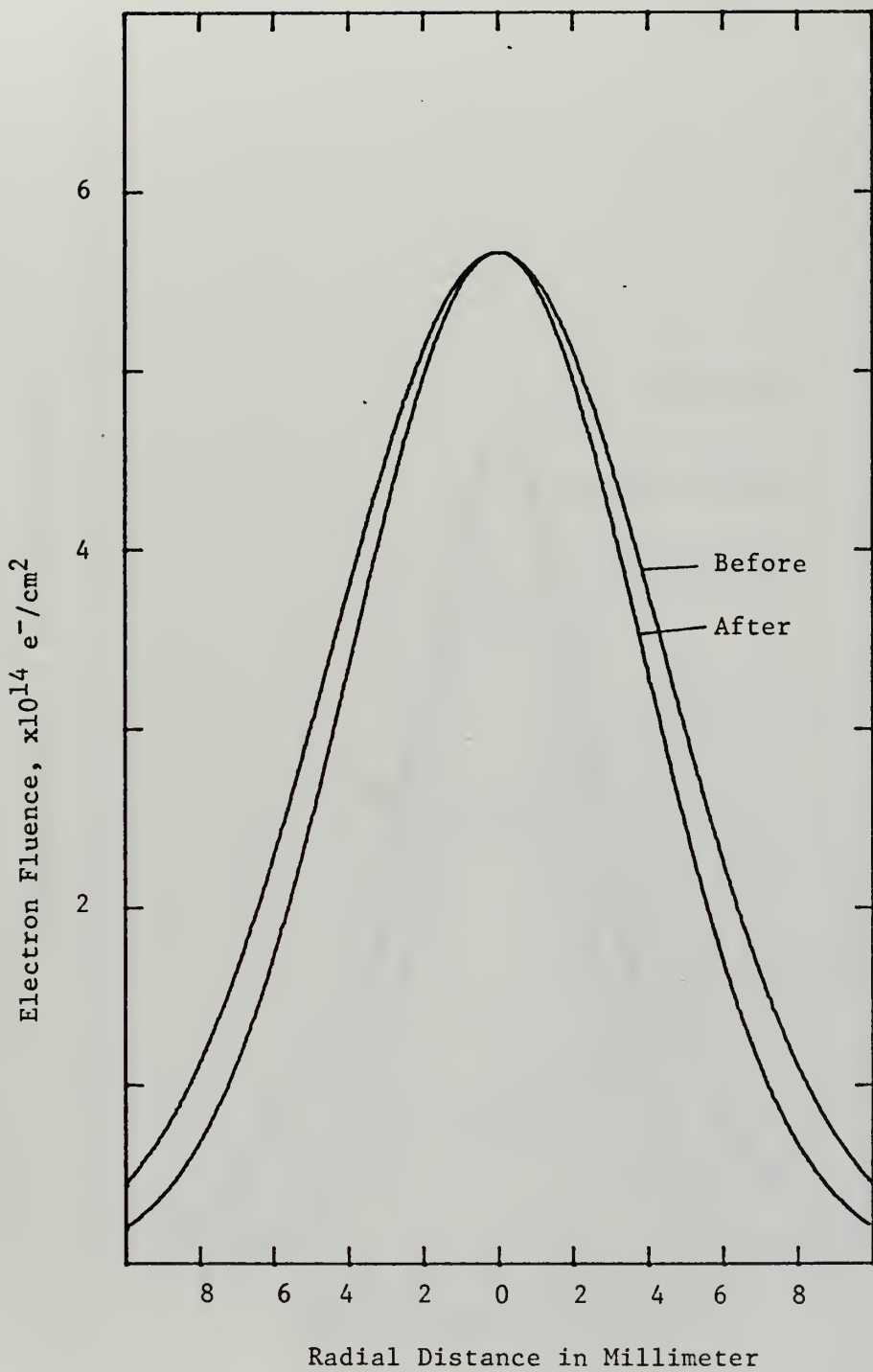


Figure 22. Beam Profiles Before and After Beryllium Slab, 25 MeV

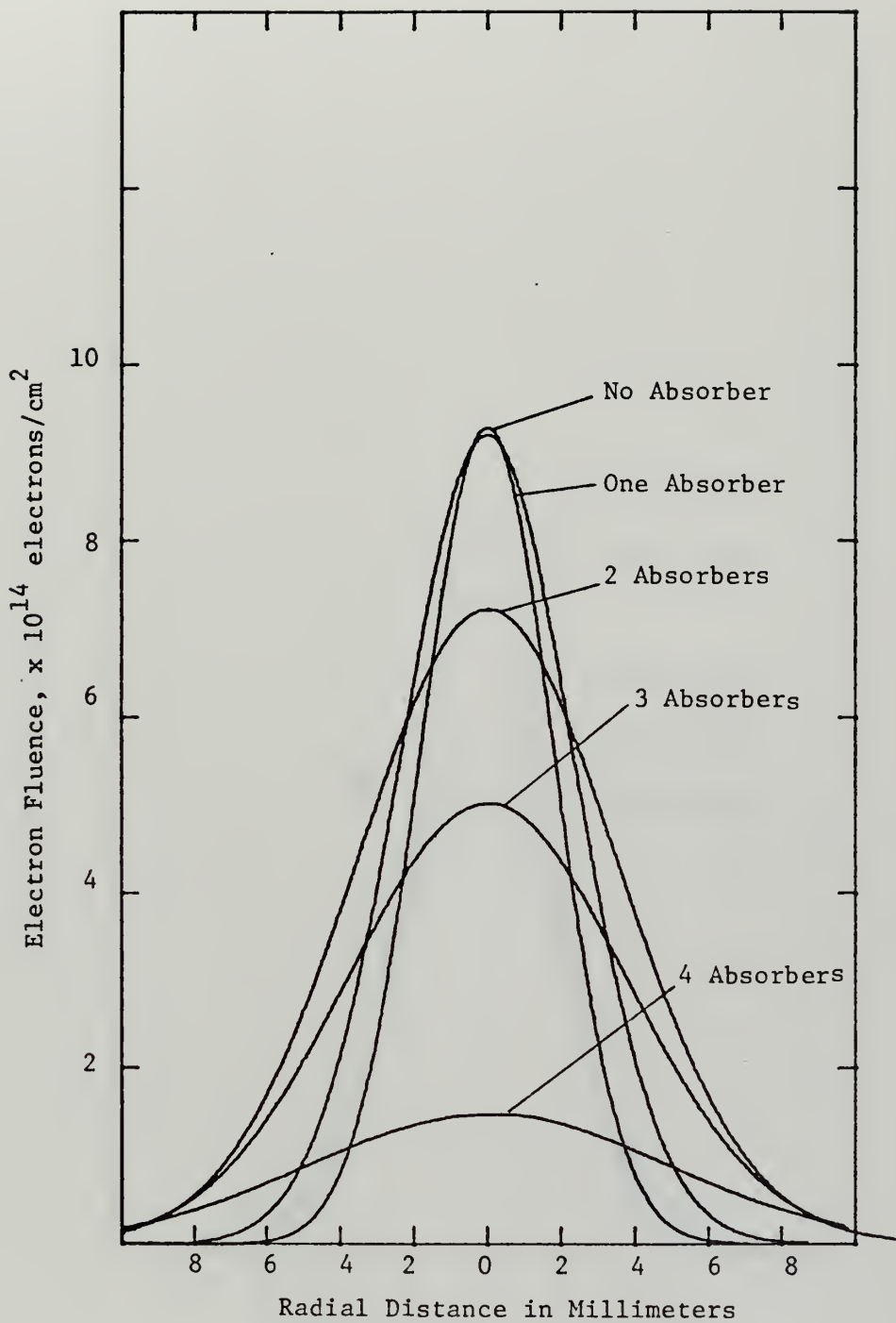


Figure 23. Beam Profiles Produced in Lead Stack 63 MeV
(Each Absorber .13" thick).

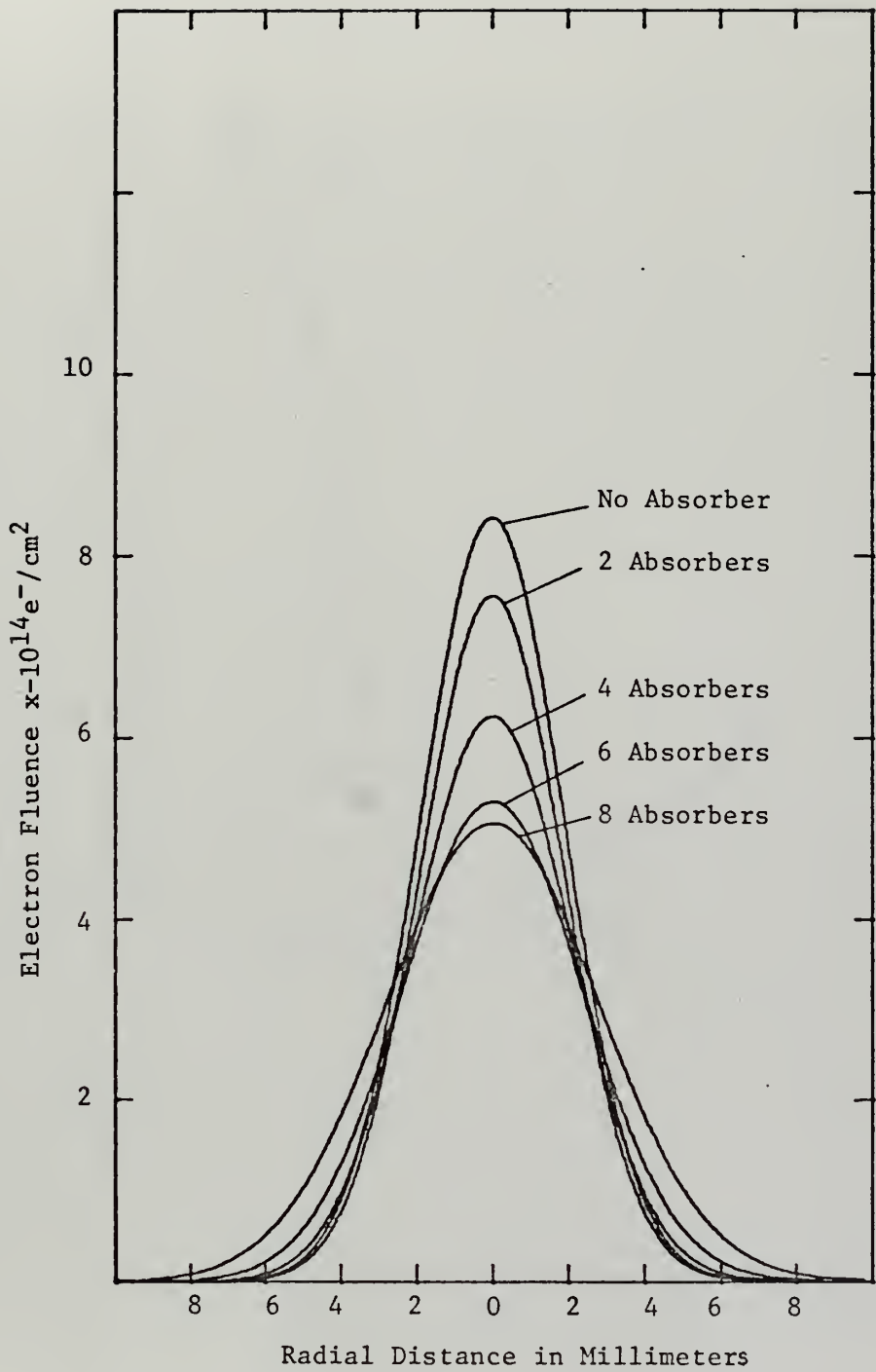


Figure 24. Beam Profiles Produced in Beryllium Stack, 63 MeV
(Each absorber .16" in thickness)

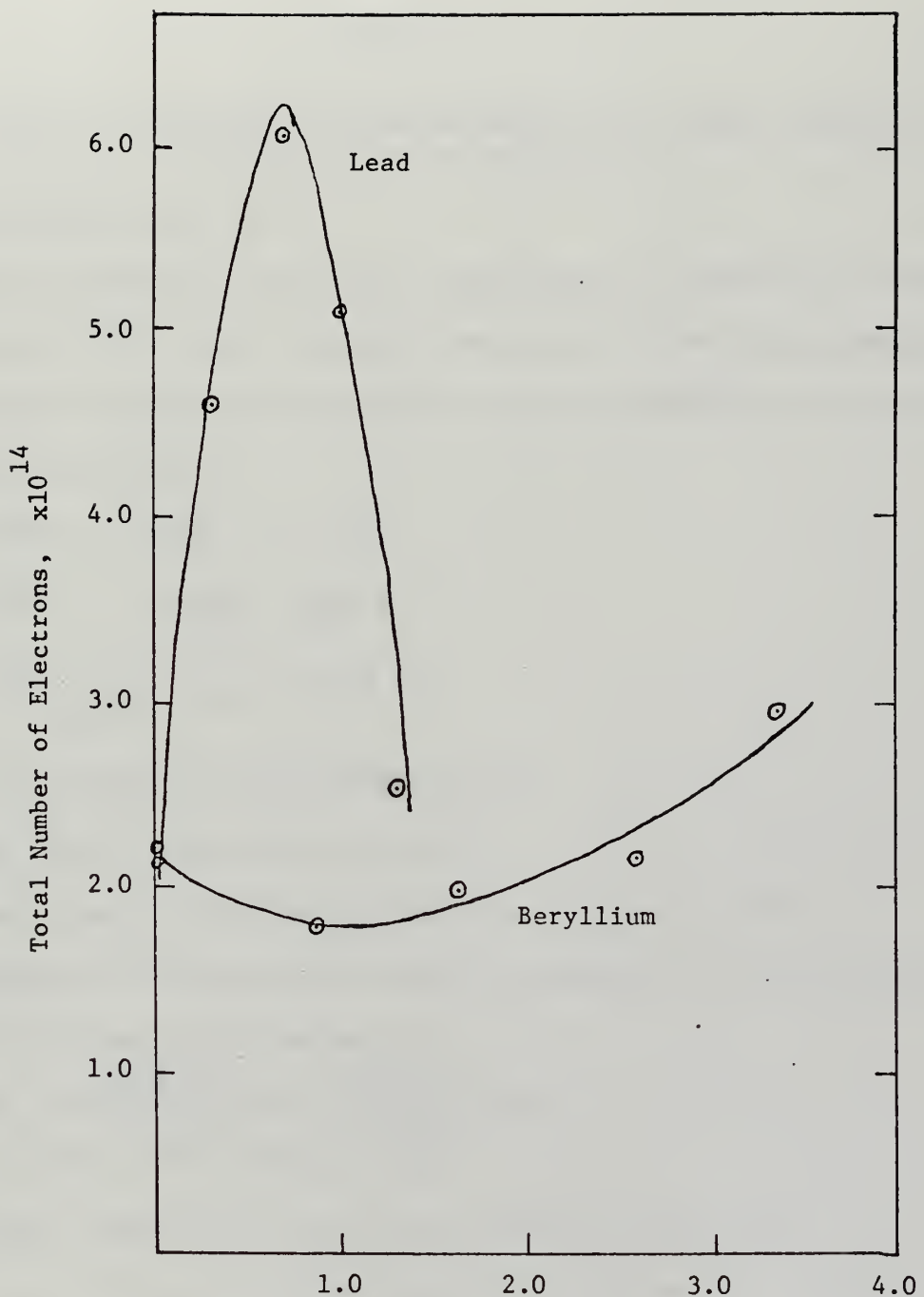


Figure 25. Effects of Absorber Thickness on Total Electrons

APPENDIX A.

DETERMINATION OF THE EFFECT OF BREMSSTRAHLUNG IN THE TARGET CAUSING PAIR PRODUCTION IN THE SEM FOILS

From Heitler [Ref. 18]

Using the extremely relativistic approximation, ignoring the effects of screening by the atomic electrons, and using the Born approximation, the formulas for the cross-sections for radiation production and pair production are given as:

$$\phi_{\text{rad}} = 4 \left(\ln \frac{2E_0}{\mu} - \frac{1}{3} \right) \bar{\phi}$$

$$\phi_{\text{pair}} = \frac{28}{9} \ln \frac{2h\nu}{\mu} - \frac{218}{27} \bar{\phi}$$

where: $\bar{\phi} = \frac{r_0^2 Z^2}{137} = 0.423 \times 10^{-29} Z^2$

E_0 = energy of the primary electron

μ = mc^2 for electron = .51 Mev

$h\nu$ = energy of emitted photon, here taken to be $1/2E_0$.

The number of electrons and positrons produced for a given electron fluence F is given by the expression:

$$N_p = 2F \left[\frac{N_0 \rho_c t_c}{A_c} \right] \times \phi_{\text{rad}} \times \left[\frac{N_0 \rho_{AL} t_{AL}}{A_{AL}} \right] \phi_{\text{pair}}$$

where $N_0 = 6.02 \times 10^{23}$ atoms per mole

ρ_c , ρ_{AL} = densities of carbon and aluminum, respectively

t_c , t_{AL} = thickness of carbon target and aluminum foil (total)

A_c , A_{AL} = atomic weight of carbon and aluminum.

N_p = number of electrons and positrons produced.

The results of this formulation, assuming no scattering of the photon beam produced by the bremsstrahlung interaction, assuming a mono-energetic photon beam of energy $1/2E_0$, are:

For 20 MeV, $N_p = (1.16 \times 10^{-6})F$

For 60 MeV, $N_p = (3.0 \times 10^{-6})F$

The accuracy of these results is certainly suspect, but should not deviate from the true results by more than an order of magnitude.

APPENDIX B

TABLE OF GAUSSIAN PARAMETERS OBTAINED BY CURVE FITTING OR BEAM PROFILES

Data was fit to the form $OD = A \exp(-x^2/\sigma^2)$

Volume $V = \pi \sigma_H \sigma_V A$

n = total number of electrons

63 Mev

Film	Location	n	Section	A	$n/V \times 10^{14}$	
1	Target Plane	3.1×10^{12}	H	.274	.066	4.69
			V	.185		
2	Target Plane	1.9×10^{12}	H	.178	.057	3.33
			V	.276		
3	Target Plane	6.25×10^{11}	H	.127	.020	3.12
			V	.245		
4	Exit Window	6.25×10^{13}	H	1.46	3.10	2.01
			V	1.78		
5	Rad Damage	1.9×10^{14}	H	3.29	11.43	1.66
			V	3.67		
6	Rad Damage	2.2×10^{14}	H	3.54	10.73	2.05
			V	3.14		
7	Rad Damage	2.2×10^{14}	H	3.40	11.99	1.83
			V	3.05		
8	Rad Damage	2.1×10^{14}	H	2.56	9.66	2.28
			V	2.60		
9	Rad Damage	2.1×10^{14}	H	2.68	9.73	2.16
			V	2.78		

Film	Location	n	Section	A	V	n/v
10	Rad Damage	4.6×10^{14}	H	5.34	.247	23.00
			V	5.50	.251	
11	Faraday Cup	1.9×10^{14}	H	5.47	.47	14.67
			V	5.40	.167	
25 MeV						
12	Target Plane	6.2×10^{12}	H	0.43	.333	0.276
			V	0.71	.245	
13	Exit Window	1.9×10^{14}	H	2.81	.417	6.01
			V	1.72	.375	
14	Rad Damage	6.6×10^{14}	H	5.49	.283	24.6
			V	5.03	.288	
15	Rad Damage	6.6×10^{14}	H	6.45	.196	24.8
			V	6.33	.192	
16	Faraday Cup	5.6×10^{14}	H	11.3	.33	43.6
			V	9.3	.13.	

LIST OF REFERENCES

1. Bess, L., Ovadia, J., and Valassis, J., "External Beam Current Monitors for Linear Accelerators," The Review of Scientific Instruments, v. 30, No. 11, p. 985-988, November 1959.
2. Gardiner, S. N., Matthews, J. L., and Owens, R. O., "An Accurate Non-Intercepting Beam Current Monitor for Pulsed Accelerator Beams," Nuclear Instruments and Methods, v. 87, p. 285-290, 1970.
3. Pruitt, J. S., "Electron Beam Current Monitoring System," Nuclear Instruments and Methods, v. 92, p. 285-297, 1971.
4. Baroody, E. M., "A Theory of Secondary Electron Emission from Metals," Physical Review, v. 78, No. 6, p. 780-787, 15 June 1950.
5. Fermi, E., "The Ionization Loss of Energy in Gases and Condensed Materials," Physical Review, v. 57, p. 485-493, 15 March 1940.
6. Halpern, O. and Hall, H., "The Ionization Loss of Energy of Fast Charged Particles in Gases and Condensed Bodies," Physical Review, v. 73, No. 5, P. 477-486, 1 March 1948.
7. Vanhuyse, V. J. and Van de Vijver, R. E., "Efficiency of Secondary Emission Monitors for Electron Beams," Nuclear Instruments and Methods, v. 15, p. 63-69, 1962.
8. Blankenburg, S. A., Cobb, J. K., and Muray, J. J., "Secondary Emission from Thin Metal Foils Bombarded with 70 MeV Electrons," IEEE Transactions on Nuclear Science, v. p. 935-941, June 1965.
9. Bumiller, F. A. and Dally, E. B., Reliability of Beam Monitors, paper presented at the International Conference on Instrumentation for High Energy Physics, Berkeley, 1960.
10. Dell, G. F. and Fotino, M., The CEA Secondary Emission Monitors, Cambridge Electron Accelerator Laboratory Publication CEAL - 1045, 4 November 1968.
11. Garwin, E. L. and Dean, N., Method of Stabilizing High Current Secondary Emission Monitors, paper presented at the Symposium on Beam Intensity Measurement, Daresbury, England, April, 1968.
12. Isabell, D. B. and Roy, P., Factors Influencing the Stability of Secondary Emission Monitors, paper presented at the 1962 International Conference on Instrumentation for High Energy Physics, C.E.R.N., July 1962.

13. Scott, M. B., Hanson, A. O., and Lyman, E. M., "Electron-Electron Scattering at 15.7 MeV, "Physical Review, v. 84, No. 4, p. 638-643, 15 November 1951.
14. Shatas, R. A., Marshall. J. F., and Pomerantz, M. A., "Dependence of Secondary Electron Emission upon Angle of Incidence of 1.3 MeV Primaries, " Physical Review, v. 102, No. 3, p. 682-686, 1 May 1956.
15. Tautfest, G. W., and Fechter, H. R., "A Nonsaturable High Energy Beam Monitor," The Review of Scientific Instruments, v. 26, No. 2, p. 229-231, February 1955.
16. Vanhuyse, V. J., and others, "Secondary Emission Beam Monitors for 0.5 - 3.5 MeV Electrons, " Nuclear Instruments and Methods, v. 15, p. 59 - 63, 1962.
17. Yount, D., A High Precision Faraday Cup and Quantameter for SLAC, paper presented at the Symposium on Beam Intensity Measurement, Daresbury Nuclear Physics Lab., Daresbury, England, April 1968, (SLAC PUB-395, Stanford Linear Accelerator Center, March 1968).
18. Heitler, W., The Quantum Theory of Radiation, 3rd Edition, Oxford, 1954.
19. Rossi, B., High Energy Particles, Prentice-Hall, 1952.
20. Humphreys, K. C. and Wilcox, R.l., Radiachromic Materials Dosimetry Study, EG&G Corporation Report, A70-28, 1970.
21. Humphreys, K. C. and Wilcox, R. L., Radiation Dosimetry and Rate Effects, EG&G Corporation Report, A69-04, 1969.
22. Attix, F. H. and Roesch, W. C., editors, Radiation Dosimetry, v. 1, Academic Press, 1968.
23. Berger, M. J. and Seltzer, S. M., Tables of Energy Loss and Ranges of Electrons and Positrons, National Aeronautics and Space Administration Report SP-3012, 1964.
24. Brown, K. L., and Tautfest, G. W., "Faraday Cup Monitors for High Energy Electron Beams," The Review of Scientific Instruments, v. 27, No. 9, p. 696-702, September 1956.
25. Charlesby, A., Atomic Radiation and Polymers, Pergamon Press, 1960.

INITIAL DISTRIBUTION LIST

No. Copies

1. Defense Documentation Center 2
Cameron Station
Alexandria, Virginia 22314
2. Library, Code 0212 2
Naval Postgraduate School
Monterey, California 93940
3. Professor J. N. Dyer, Code 61Dy 1
Department of Physics
Naval Postgraduate School
Monterey, California 93940
4. Assoc. Professor E. B. Dally, Code 61Dd 1
Department of Physics
Naval Postgraduate School
Monterey, California 93940
5. CAPT Frederic C. Gray 1
919 N. Highland Street
Arlington, Virginia 22201

DOCUMENT CONTROL DATA - R & D

(Security classification of title, body of abstract and indexing annotation must be entered when the overall report is classified)

1. ORIGINATING ACTIVITY (Corporate author) Naval Postgraduate School Monterey, California 93940		2a. REPORT SECURITY CLASSIFICATION Unclassified
2b. GROUP		
3. REPORT TITLE Beam Current Monitoring and Radiachromic Film Dosimetry at the NPS Linac		
4. DESCRIPTIVE NOTES (Type of report and, inclusive dates) Master's Thesis; June 1972		
5. AUTHOR(S) (First name, middle initial, last name) Frederic Colbert Gray		
6. REPORT DATE June 1972	7a. TOTAL NO. OF PAGES 64	7b. NO. OF REFS 25
8a. CONTRACT OR GRANT NO.	9a. ORIGINATOR'S REPORT NUMBER(S)	
b. PROJECT NO.		
c.	9b. OTHER REPORT NO(S) (Any other numbers that may be assigned this report)	
d.		
10. DISTRIBUTION STATEMENT Approved for public release; distribution unlimited.		
11. SUPPLEMENTARY NOTES	12. SPONSORING MILITARY ACTIVITY Naval Postgraduate School Monterey, California 93940	
13. ABSTRACT <p>The beam current monitoring system at the NPS electron Linac was studied to determine its performance under varying conditions of machine operation. The efficiency of the secondary emission monitors (SEM Efficiency), defined as the ratio of SEM current of Faraday cup current, was found to increase with increasing beam energy, increase with the introduction of targets into the beam, and vary erratically with SEM foil surface conditions. No dependence on beam current was observed.</p> <p>The spatial variation of electron fluence (time-integrated flux) was investigated using RACM 203 radiachromic film developed by the EG&G Corporation. The optical density of this film was found to vary linearly with absorbed dose over a range of 5 to 40 megarads. Beam profiles were obtained at 4 locations in the Linac end station for beam energies of 25 and 63 MeV. In addition, the film was used to observe and measure the effect of cascade showers in thick absorbers.</p>		

14.

KEY WORDS

KEY WORDS		LINK A		LINK B		LINK C	
		ROLE	WT	ROLE	WT	ROLE	WT
Secondary Emission Monitors							
Radiachromic Films							
Electron Beam Profile							

DD FORM 1473 (BACK)

1 NOV 65

S/N 0101-807-6821

Unclassified

Security Classification

Thesis

G716 Gray

c.1 Beam current moni-
toring and radiachromic
film dosimetry at the
NPS Linac.

134719

Thesis
G716
c.1

Gray Beam current moni-
toring and radiachromic
film dosimetry at the
NPS Linac.

134719

thesG716

Beam current monitoring and radiachromic



3 2768 002 13854 7

DUDLEY KNOX LIBRARY